



Rockfall Occurrence and Fragmentation

Jordi Corominas, Olga Mavrouli, and Roger Ruiz-Carulla

Abstract

Rockfalls are very rapid and damaging slope instability processes that affect mountainous regions, coastal cliffs and slope cuts. This contribution focuses on fragmental rockfalls in which the moving particles, particularly the largest ones, propagate following independent paths with little interaction among them. The prediction of the occurrence and frequency of the rockfalls has benefited by the rapid development of the techniques for the detection and the remote acquisition of the rock mass surface features such as the 3D laser scanner and the digital photogrammetry. These techniques are also used to monitor the deformation experienced by the rock mass before failure. The quantitative analysis of the fragmental rockfalls is a useful approach to assess risk and for the design of both stabilization and protection measures. The analysis of rockfalls must consider not only the frequency and magnitude of the potential events but also the fragmentation of the detached rock mass. The latter is a crucial issue as it affects the number, size and the velocity of the individual rock blocks. Several case studies of the application of the remote acquisition techniques for determining the size and frequency of rockfall events and their fragmentation are presented. The extrapolation of the magnitude-frequency relationships is discussed as well as the role of the geological factors for constraining the size of the largest detachable mass from a cliff. Finally, the performance of a fractal fragmentation model for rockfalls is also discussed.

Keywords

Rockfalls • Magnitude-frequency relations • Fragmentation • Hazard analysis

Introduction

Rockfalls are widespread phenomena in mountain ranges, coastal cliffs, volcanos, river banks, and slope cuts. Although most of them take place in remote places, they also threaten residential areas and transport corridors (Hung

et al. 1999; Chau et al. 2003; Corominas et al. 2005). The unpredictable nature often attributed to the rockfalls events is cause of concern of the authorities and decision makers. Although rockfalls have a limited size, they are extremely rapid processes that exhibit high kinetic energies and damaging capability. Turner and Jayaprakash (2012) prepared an exhaustive list of rockfall events which demonstrates that even relatively small volumes of rocks may cause significant damage and traffic disruption, particularly in railroads. Recent studies (Petley 2012) have shown that losses due to landslides and rockfalls are concentrated in less developed countries in which deficit of research exists, and often lack of the appropriate resources.

This type of events may be mitigated with stabilization and protection works but often engineers have to make

J. Corominas (✉) · O. Mavrouli · R. Ruiz-Carulla
Department of Civil and Environmental Engineering, Universitat
Politécnica de Catalunya, Jordi Girona 1-3, 08034 Barcelona,
Spain
e-mail: Jordi.corominas@upc.edu

O. Mavrouli
e-mail: olga.mavrouli@upc.edu

R. Ruiz-Carulla
e-mail: roger.ruiz@upc.edu

difficult judgements due to the uncertainties associated to the prediction of the size and frequency of the potential events.

Rockfalls are defined as the detachment of a rock from a steep slope along a surface on which little or no shear displacement takes place (Cruden and Varnes 1996). The main feature is that the mass descends very rapidly through the air by falling, bouncing, and rolling. Furthermore, almost no interaction takes place between the most mobile moving fragments, which interact mainly with the substrate (Hungre et al. 2014). Rockfalls are considered relatively small mass movements confined to the detachment of an individual rock or a relatively small rock mass (Selby 1982). Detachments of large-scale rock masses are defined as rockslides and rock avalanches (Cruden and Varnes 1996).

It is widely accepted that rockfalls and rock avalanches exhibit different propagation mechanisms. However, there is still a debate on the characterization of rockfalls, particularly on their dimensions. Some researchers attempted to restrict the term rockfall based on a maximum kinetic energy (Spang and Rautenstrauch 1988) or on volumetric terms such as debris falls ($<10 \text{ m}^3$), boulder falls ($10\text{--}100 \text{ m}^3$), block falls ($>100 \text{ m}^3$), cliff falls ($10^4\text{--}10^6 \text{ m}^3$) and Bergsturz ($>10^6 \text{ m}^3$) (Whalley 1984). The current practice indicates that terms such as rockfalls, rockslides and rock avalanches are often used in a non-coincident way (i.e. Hungre et al. 1999; Chau et al. 2003; Dussauge-Peisser et al. 2002; Guzzetti et al. 2003) and that the agreement on the terms has not yet reached. Turner and Jayaprakash (2012) found preferable to maintain the definition of rockfall as one involving significant velocities and some measure of free flight without an upper limit on the volume or kinetic energy of individual blocks. An interesting consideration was made by Rochet (1987), who distinguished between stone fall (chute de pierre) up to few hundred of cubic meters, in which no interaction exists between the rock fragments which follow independent trajectories; rock mass fall (éboulement en masse) up to few hundreds of thousands of cubic meters in which the interaction between particles is weak as they follow independent trajectories or soon they become independent; very large rock mass fall ($>10^5\text{--}10^6 \text{ m}^3$) showing strong interaction of particles within the moving mass with the development of internal pressures (possible fluidification) and low energy dissipation; mass propagation (déplacement en masse) ($>10^6 \text{ m}^3$) that progresses mostly by a translational displacement. Evans and Hungre (1993) introduced the term fragmental rockfall to describe the events in which the individual fragments move as independent rigid bodies interacting with the substrate by means of episodic impacts. They usually involve volumes smaller than 10^5 m^3 . For larger volumes, the blocks propagate as granular flows and are considered rock avalanches (Hungre et al. 2014). Distinguishing between these terms is relevant because fragmental rockfalls are modelled by means of

ballistic trajectories while rock avalanches are simulated as granular flows (Bourrier et al. 2013). The passage from a falling of independent particles to a granular flow is gradual and both mechanisms can coexist in some events. The transition may take place at volumes as small as $5 \times 10^4 \text{ m}^3$ (Davies and McSaveney 2002) although other authors raise it up to 10^7 m^3 (Hsü 1978). In light of these considerations, in the authors' opinion it is preferable not to propose a specific volume threshold between them as suggested by Turner and Jayaprakash (2012). This communication will focus on fragmental rockfalls only.

Large rockfalls, rockslides and rock avalanches are sometimes difficult to distinguish one from the other (Chau et al. 2003). Rockfall affected areas are characterized by the presence of scars at the rock face and by the presence of rock blocks scattered over the slope, which are less evident if the vegetation cover is present. In case of very active rock walls, the repeated fall of rock fragments generates a talus deposit at the foot of the slope, in which the segregation of blocks by volume takes place. Fine material is found near the apex while the mean block size increases downslope (Evans and Hungre 1993). This sorting is consequence of the lesser kinetic energy of the small rock blocks, which can be easily stopped by obstacles and trapped in depressions between larger rocks of the talus slopes (Statham 1976; Dorren 2003). As the size of the falling mass increases, blocks located underneath the mass during the impact may become crushed, generating a large amount of minor particles.

Rock avalanches are expected to travel far beyond the distal edge of the talus slopes (Wieczorek 2002). The generated debris sheet often spreads in the direction transverse to the flow and has a chaotic arrangement in which huge blocks define an extremely irregular, rough morphology (Soeters and Van Westen 1996). The drainage pattern may be seriously disturbed and the accumulated mass may be large enough to dam the stream and generate a lake. Lobate shapes and either longitudinal or transverse ridges are often found, sometimes close to the front of the deposit (Hewitt 1999; Hewitt et al. 2008). The debris is composed of crushed and pulverized rock and contains the same lithology from the largest blocks up to the smallest ones. In case several lithotypes are involved they maintain their identity and form bands that respect the original stratigraphic order (Davies et al. 2009; Hewitt et al. 2008).

Rockfall Source Characterization

The failure of a rock slope is controlled by the lithology, strength and structure of the rock mass. The existing discontinuities, their orientation, spacing and persistence determine the failure mechanism (i.e. planar, wedge, toppling), which can be assessed by stability analyses (Hoek

and Bray 1981). The failure of the rock mass and the onset of a rockfall depend on additional factors such as rock strength, degree of weathering, cleft water pressures, and erosion (Budetta 2004). To account for the interaction between the discontinuities and rock shearing, the conventional kinematic and limit equilibrium techniques to simulate simple failures are replaced by numerical continuum–discontinuum codes with fracture simulation capabilities, well suited to complex instabilities (Eberhardt et al. 2004). The latter requires effective data collection in the field and data interpretation for potential failure modes.

The characterization of the rock mass fracture pattern has traditionally been carried out in the field, with systematic sampling of discontinuities. The most rigorous way is by scanlines (Priest and Hudson 1981; Priest 1993), for which the distribution function of the different joint sets and their spacing is obtained. This procedure, performed in situ has obvious limitations due to the inaccessibility of the outcrops (especially in steep cliffs), high time consumption for data collection and the possibility of measurement errors. Modern techniques allow us to characterize the structure visible from a remote and safe position. The LiDAR technology has experienced rapid expansion and growing with multiple applications in architecture, science and engineering (Heritage and Large 2009). Equipment mobility, accuracy and data acquisition rate, compared to conventional surveying and photogrammetric methods, permits an unprecedented level of detail and is useful for geotechnical purposes. The ability to remotely capture the position of the points on the exposed rock and its processing has significant advantages ranging from safety to efficiency, resulting in a high resolution record.

The advances in techniques of data capture have contributed of the development of methodologies that exploit these high-resolution data in the domain of the structural geology and rock mechanics. These include the generation of high resolution Digital Surface Models (Slob et al. 2002; Kemeny et al. 2006; Jaboyedoff et al. 2007), the identification and characterization of discontinuity sets (Kemeny and Post 2003; Sturzenegger and Stead 2009a, b; Slob et al. 2004; Jaboyedoff et al. 2009; Riquelme et al. 2014), the measurement of the spacing of the joint sets (Slob 2010; Oppikofer et al. 2011; Riquelme et al. 2015) or the definition of potentially movable rock masses (Lato et al. 2009). In the following sections some applications of the use of Lidar, also in combination with digital photogrammetry for analysis of the rockfalls, will be presented.

The laser scanner equipment can be terrestrial (TLS) or mounted on an aircraft (airborne-based or ALS). The operation of the LiDAR equipment for data acquisition and software packages for processing are becoming more affordable. It generates a large database of points defined by the coordinates x, y, z (3D point cloud). The capture rate

ranges from 2500 to 500,000 points per second, depending on the type of scanner used and allows creating scenes. To build the point cloud it is required several scans from different points of view, which will be aligned with each other. This is done to avoid occlusion of the points and to increase the density of the point cloud (Jaboyedoff et al. 2012).

The ability to convert a set of points of known positions, as the compiled by the LiDAR, in a database of structural measures, requires several phases (see details in Jaboyedoff et al. 2012). Points must be collected and processed, then manipulated and analyzed for characterization. Data processing should be done with knowledge of the structure to be analyzed. To identify a particular surface in the point cloud, the number of captured points must be sufficient for it to be displayed. This value depends on the extent of the visible surface, and the density of points that can be acquired, which in turn depends on the distance from the recognized surface and the beam divergence of specific equipment. The more variable orientation of the surface or larger the roughness, the more the data density are required.

The TLS still has limitations in the viewing distance and the emergence of areas of occlusion when the escarpment has large vertical development or in the case of rock protrusions (Sturzenegger and Stead 2009b). Some of these restrictions may be overcome by combining TLS/ALS with digital photogrammetry. This technique allows the production of 3D point clouds from a set of photographs taken of the object of interest. It also allows the generation of meshes that are texturized with the same images, obtaining 3D models for the characterization of geological 3D structure (Lim et al. 2005; Sturzenegger and Stead 2009b). The photographs necessary for the use of digital photogrammetry must have enough quality and can be taken from the ground or from the air. The digital photogrammetry reaches its highest potential when the camera is mounted on an Unmanned Aerial Vehicle (UAV or drone). It carries navigation and inertial systems (gyroscopes, accelerometers, altimeters and GPS) and may perform flights of predefined trajectories of a rock face. The use of UAVs offset the lower image resolution with a closer approach to the rock face safely and different angles of observation. The reader will find more details about the performance, applications and limitations of these techniques in several review papers and in the references therein (Wehr and Lohr 1999; Haneberg 2008; Jaboyedoff et al. 2012).

Rockfall Prediction

The temporal prediction of the slope failure has been traditionally the weakest point in the rockfall hazard analysis and management. For long time, rockfalls were assumed as the sudden detachment of a rock mass from a cliff but they are

not. Successive Lidar data captures and DinSAR images have demonstrated that the progressive deformation of the slope takes place before failure.

Failure of rock masses is frequently preceded by creep, progressive deformation, and extensive internal disruption of the slope mass (Stead et al. 2006). The prediction of time to failure can be based on measurements of either surface or subsurface displacements, repeated over time (Hungri et al. 2005). This approach does not take necessarily into account the underlying mechanism of failure and concentrates on the evolution of the slope face. It was first proposed by Saito (1965) and later developed by Voight (1989) and Fukuzono (1990). Plotting the inverse displacement rate versus time generates trend-lines that are projected considering different rheological creep models to the zero value on the abscissa (time axis) and calculate the failure time. The practical application of these methods to failure prediction requires that velocity threshold values be set. It is worth noting that the interpretation of these trends is sometimes difficult due to the fluctuation of the external slope conditions (i.e. rainfall), that may induce deviations of the rate of displacement. Comprehensive discussion and reviews of these methods are provided by Petley et al. (2002), Crosta and Agliardi (2003), Rose and Hungri (2007).

Nowadays, the monitoring of slope movements has become standard practice in most mining and geotechnical projects. Slope displacements as well as other visual precursors such as cracking, localized falls, audible noise are recorded to predict the time of failure. Techniques such as the LiDAR equipment, digital photogrammetry and radar interferometry provide not only the analysis temporal patterns of the precursors before a large slope failure but also the spatial one, thus allowing the definition of the size of the unstable volumes (Oppikofer et al. 2008; Ferrero et al. 2011; Stock et al. 2012; Royán et al. 2014, 2015). Periodic surveys using TSL have shown an increase of the rate of small-size rockfall events prior to the failure of large masses, which are mostly concentrated in the detachment zone (Rosser et al. 2007; Royán et al. 2014; Kromer et al. 2015). The above observations are accompanied with an increase in the displacements of the moving mass away from a background level. The larger the volume of the unstable mass the sooner and greater the number of these features noticed (Rosser et al. 2007).

Although several uncertainties remain associated on whether every large rockfall has precursors and to the determination of the exact time of failure using the creep curves, the measurement of the slope displacements which may be analyzed in combination with other indicators (Amitrano et al. 2005), enables the identification of potential catastrophic failures, so that future events can be recognized beforehand and the society can adapt to the hazard (Gischig et al. 2009; Hermanns et al. 2013).

Rockfall Risk Assessment

The land-use planning and the safety of the transportation corridors require the appropriate analysis of the rockfall hazard. This task is facilitated by the Quantitative Risk Analysis (QRA) approach. It is a powerful management tool in which assumptions and uncertainties are explicitly expressed and considered (Fell et al. 2005). QRA facilitates the objective decision making as it eliminates the use of ambiguous terms, the results are repeatable and consistent, and provides the ingredients for cost-benefit analysis for different scenarios (Corominas and Mavrouli 2011; Corominas et al. 2014). QRA in rockfalls, requires the determination of the probability of the slope failure for a range of volumes; the expected trajectories and the fragmentation of the detached mass, and the evaluation of the probability of impact and damage to the exposed elements. As the available information is often limited, Lee and Jones (2004) warned that the probability of the slope failure and the value of adverse consequences are only estimates.

The risk for a given rockfall location may be expressed analytically as follows (modified from Corominas et al. 2014):

$$R = \sum_{M_i} P(M_i)P(X_j|M_i)P(T|X_j)V_{ij}C \quad (1)$$

Where

R	Risk due to the occurrence of a rockfall of magnitude M_i on an element at risk located at a distance X from the landslide source
$P(M_i)$	Probability of occurrence of a rockfall of magnitude M_i
$P(X_j M_i)$	Probability of the rockfall reaching a point located at a distance X from the landslide source with an intensity j
$P(T X_j)$	Probability of the element being at the point X at the time of the rockfall occurrence
V_{ij}	Vulnerability of the element being impacted by a rockfall of magnitude i and intensity j
C	Value of the element at risk

The rupture of the rock wall and its probability $P(M_i)$ define the rockfall initiation and is the most challenging part of the rockfall hazard assessment. The potential for failure can be approached from either rational (geomechanical approach) or empirical methods.

Rational Approach

In the geomechanical approach, the stability of the slope can be evaluated using analytical tools (Hoek and Bray 1981) or numerical calculation considering the strength of the rock

mass (Eberhardt 2008; Stead et al. 2006). The geomechanical analysis is the appropriate tool for the understanding of the underlying mechanisms driving the instability. The assignment of the properties of the rock mass (rock strength, water pressure, joint orientation and persistence, among others) is however subjected to a high degree of uncertainty.

The classical result of the slope stability analysis is the Factor of Safety, which is only a qualitative expression of the probability of failure. The latter may be addressed using probabilistic slope stability analyses which incorporate and quantify the uncertainties associated to the variability of the input parameters by means of their statistical distributions (El-Ramly et al. 2002). It must be noted that the statistical analyses should be based on sufficient amount of data, otherwise they can be misleading. If data are sparse, a simplified analysis using both the most likely parameters' values and the most unfavorable ones is preferable (Hungri 2016).

Even though the outputs of these methods can be implemented on GIS platforms and may be used to prepare maps showing the potential for rockfall failure from a source area, time is not explicitly taken into account and because of this, they are not currently used in hazard analyses and zoning. Furthermore, procedures for the estimation of the model parameters values at regional scale have yet to be developed.

Frequency Analysis

The empirical methods calculate the probability of failure by statistical analysis using inventories of past events, which also allow preparing magnitude-frequency (MF) relations of the events (Hungri et al. 1999; Dussauge-Peisser et al. 2002; Guzzetti et al. 2003).

It must be taken into account that landslides do not repeat themselves. Despite of this, rockfalls as well as debris flows are landslide types that are usually treated as repetitive events (Corominas and Moya 2008). The temporal occurrence of landslides may be expressed in terms of frequency, return period, or exceedance probability. The frequency expresses the number of events in a certain time interval (e.g. annual frequency) and it can be assessed from the rockfall inventories.

The statistical analyses applied to landslides have found that magnitude versus the cumulative number or frequency of landslides is scale invariant and follows a power law distribution (Hovius et al. 1997; Pelletier et al. 1997; Guzzetti et al. 2002b). The size distribution is similar to the observed by Gutenberg and Richter for earthquakes, and may be expressed in the following way:

$$\text{Log}_{10}N(> M) = a - bM \quad (2)$$

Where N is the cumulative number of landslides greater than magnitude M ;

While “ a ” and “ b ” are coefficients. “ a ” is a measure of the level of landslide activity; and “ b ” is the gradient of the relation, where higher b -value indicates a larger proportion of small landslides, and lower b -value a smaller proportion of small landslides. As M is measured on a logarithmic scale, then a linear relationship is obtained in the log-log scale.

This type of relations have been obtained for debris flows (Guthrie and Evans 2004; Hungri et al. 2008) and rockfalls (Hungri et al. 1999; Dussauge-Peisser et al. 2002; Chau et al. 2003; Guzzetti et al. 2003). In order to perform this analysis it is required an inventory as complete as possible (Hungri et al. 1999; Dussauge-Peisser et al. 2002).

The TLS has been used for the identification and calculation of volumes of rock blocks that have fallen, from the images of sequential scans (Abellan et al. 2006; Royán et al. 2015). The subtraction of the Digital Surface Models (DSM) obtained with the respective point clouds can accurately calculate the missing volumes. If the geometry prior to the failure is unknown, the volumes disappeared can be calculated by the reconstruction of the original topography on a DSM generated based on earlier pictures of the event. Oppikofer et al. (2009) detected scars on a rocky wall surfaces formed by the failure and reconstructed the original relief by fitting discontinuity planes to the scars, using specific programs and limited number of scars. Unfortunately, rockfall inventories are not always available or are incomplete. Most historical records cover a limited period while the TLS equipment has been available for only the last few years. This may lead to obviate the occurrence of large infrequent failures.

For landslide risk management purposes, one of the most important questions to answer is what the likelihood of infrequent events is. In that respect several questions arise about the validity of the obtained power laws in both space and time domains and whether they can be extrapolated or not. Dussauge-Peisser et al. (2002) discussed the interpretation of the fitting parameters a and b -values. They consider that if the data do not fit any law, the inventory can be used to estimate an overall frequency in the range of volumes covered by the data. However, in case a power law can be fitted and statistical tests certify the completeness, then it is possible to extrapolate the frequency to larger volumes. This point of view is shared by other researchers (Guzzetti et al. 2003; Picarelli et al. 2005). In any case, as noted by Corominas and Moya (2008) the frequency-magnitude relation for landslides is not purely linear in a log-log scale. A rollover effect (a flattening of the curve) is observed at small landslide magnitudes. This implies that the number of observed small size landslides, is lower than the one

expected from the above relationship. It has been suggested that rollover might be due to the incompleteness (censoring) of landslide records because small landslides are not detected in aerial photographs (Hungri et al. 2008; Stark and Hovius 2001) or that some kind of physical constraint must exist that justifies this rollover at small sizes (Guthrie and Evans 2004). However, the lack of fit to the power law may also take place at large landslide magnitudes (Guzzetti et al. 2002b; Malamud et al. 2004) and, consequently other causes should be explored in order to explain such behavior. These types of constraints are not well understood yet. This issue becomes critical when dealing with rockfall risk management strategies.

Obtaining the Distribution of Missing Volumes in Cliffs

Obtaining long records of rockfalls is a challenging task because in road and railways cuts, the rock blocks are immediately removed after their occurrence in order to resume the traffic conditions. In some exceptional cases, the maintenance teams have collected the necessary information for the preparation of MF relations (Hungri et al. 1999; Ferlisi et al. 2012). Unfortunately, the situation is worse in natural slopes. A few number of historical rockfall inventories are available that allow the analysis to the scale of up to a hundred years (Wieczorek et al. 1998; Guzzetti et al. 2003; Hantz et al. 2003). On the other hand, the rock blocks deposited at the slope below the rockfall sources cannot be usually used to prepare data sets because it is not possible to discriminate which of the blocks belong to the different rockfall events that have generated the deposit.

Instead, the cliff face where the rockfalls have been generated may keep the record of the events occurred during the last hundreds or thousands of years in the form of rockfall scars. The scar is an area of rupture on the rock wall or cliff, generated by the separation of a rock mass in a single or multiple events (Fig. 1). The distribution of volume or density of scars, are indicative of the occurrence of rockfalls and can be used as an indirect measure of the frequency of the events.

We have developed a supervised and stepwise methodology for calculating the volume distribution of rockfall scars using the TLS. This section summarizes the work carried out in the steep and intensely fractured granodiorite rock wall of Forat Negre in the Solà de Santa Coloma, Principality of Andorra (Santana et al. 2012). In the last decades buildings were built in the Solà de Santa Coloma and are threatened by rockfalls. The talus deposit at the

bottom of the slope contains blocks with volumes between 0.5 and 270 m³. The detailed description of the area and the actions undertaken protection are found at Copons (2007), Copons et al. (2004), or Corominas et al. (2005).

The input data are the point clouds from which the planes present in the slope surface are extracted, the main discontinuity sets are identified, the area of the exposed surfaces of each of the scars are calculated, their height as well and finally the distribution of rock volumes that have disappeared from the wall is calculated. The analysis is based on several assumptions (Santana et al. 2012): (i) the detachment of the rock blocks at a particular point is due to the presence of unfavorable dipping discontinuities and/or its intersection with other discontinuities; (ii) the volume of the scars is approached by a prism formed by the intersection of discontinuities in the rock wall, as shown in Fig. 2; (iii) each scar basal plane corresponds to at least one rockfall event; and (iv) the detachment over adjacent sliding surfaces with the same orientation, but separated by a step of at least 20 cm jump are considered independent events. According to these assumptions, step-path failures are taken into consideration but only for steps smaller than 0.2 m.

The analysis of the point cloud allowed to identify 7 main discontinuity sets (Table 1). Kinematic analysis indicates that two sets, F3 and F5, generate potential planar failures, which is predominant failure mode for rockfalls in the study area as confirmed by the inventoried cases (Copons 2007). F1 and F7 sets bound the unstable rock blocks and act as tension crack and lateral release plane, respectively. These four sets account for 78% of the discontinuities present at the rock mass (Table 1). To obtain the volume distribution of the scars, the points of the point cloud belonging to each one of the four sets F1, F3 and F5, and F7 were filtered and planes were adjusted to them. These planes correspond to the scar edges. Their areas, the maximum width (along the strike) and length (along the dip direction) were measured. The heights of the scars are defined by the intersections of the planes of joints F1 and F7, and their distribution is defined by the common length of these planes. Eventually, the size distribution of the scars was calculated by means of a Monte Carlo simulation, multiplying the scar basal areas with the heights. The scar volumes were assumed to be prismatic as the angles between the height and the basal area are greater than 60° and the inaccuracy imposed by considering angles of 90° is limited (Palmstrom 2005).

For a sample of 5000 scars, which is of the same order of magnitude as the identified scars on the point cloud, the maximum calculated scar volumes are of the order of few thousands of m³ (~3000 m³). This is the maximum rock mass size that has been detached from the slope face leaving

Fig. 1 Example of rockfall scars (*blue polygons*) observable at the Degotalls wall, Montserrat massif, Catalanian Coastal Ranges, Spain

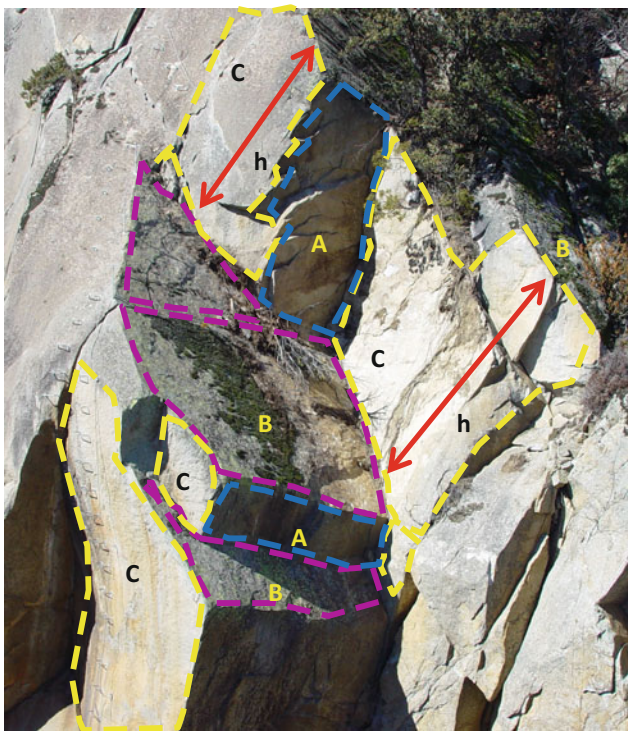
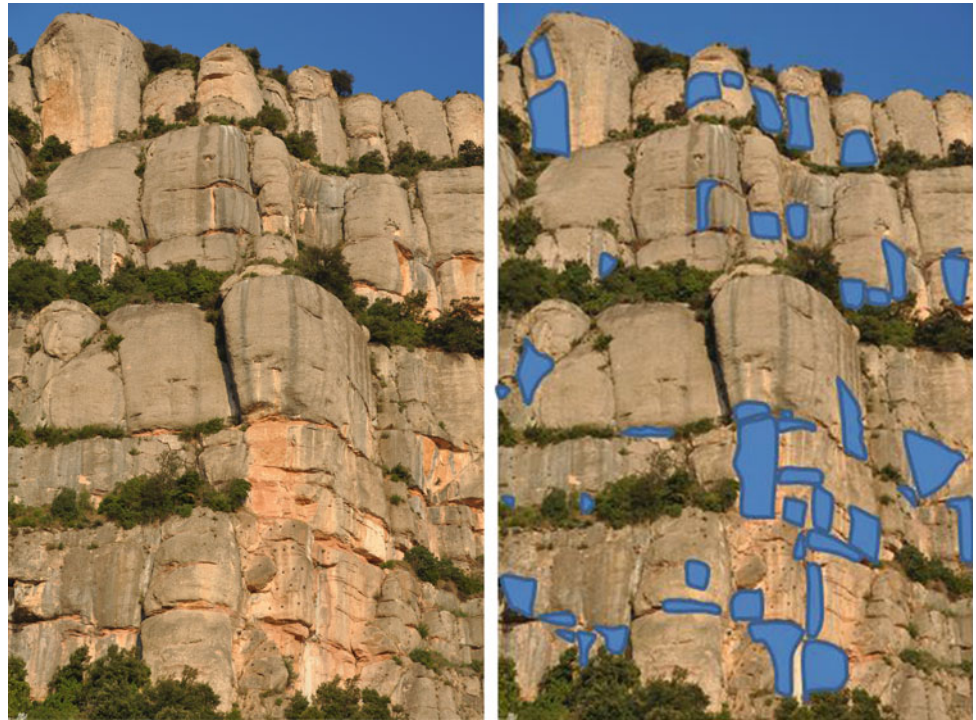


Fig. 2 Rockfall scar defined by three intersecting joint sets. The detached block was resting on a basal plane (*B*) which is bounded by planes (*A*) and (*C*). The *height* of the scar (*h*) may involve several spacings

a scar on it. The largest observed scar base was 213 m², indicating a respective scar height of the order of 15 m. The resolution of the technique allows the detection of volumes as small as 0.02 m³.

For scar volumes larger than 0.75 m³, the distribution is well fitted by the following inverse power law (Fig. 3):

$$N(v > V) = 1919v^{-0.9} \quad (3)$$

Where *N* is the accumulated number of rockfall scars larger than a volume *V*, in cubic meters

It is worth noticing that in the Solà de Santa Coloma, the occurrence of rockfalls (larger than 1 m³) during the last 50 years is one every two years as an average (Moya et al. 2010). The obtained distribution may thus represent the result of the rockfall activity in the slope for the last few thousands of years. Due to the assumption adopted, this volume distribution should be considered an upper envelop for the rockfall volumes because the scars may be the result of one or several failure events. However, this distribution might underestimate the occurrence of the largest failures because only the step-path surfaces with steps smaller than 0.2 m have been measured in the followed approach. Despite of this, neither the presence of large scarps suggesting the occurrence of any large failure nor the presence of a massive rockfall or avalanche deposits have been identified in the slope and valley bottom respectively.

Table 1 Discontinuity sets of the Forat Negre slope, relative frequency and maximum and minimum areas obtained with TLS (modified from Santana et al. 2012)

Joint set	Dip direction/angle (°)	Relative frequency (%)	Maximum area (m ²)	Minimum area (m ²)
F1	056/63	13.5	121.6	0.3
F2 ^a	320/60			
F3	155/57	25.7	236.3	0.7
F4A	247/45	1.4	11.6	0.4
F4B	266/64	2.7	20.3	0.4
F5	187/54	17.7	144.4	0.7
F6	187/75	9.1	23.8	0.5
F7	155/87	21.5	213.7	0.5
F8	092/57	4.2	34.6	0.4

^aMerged with F7 in the LiDAR analysis

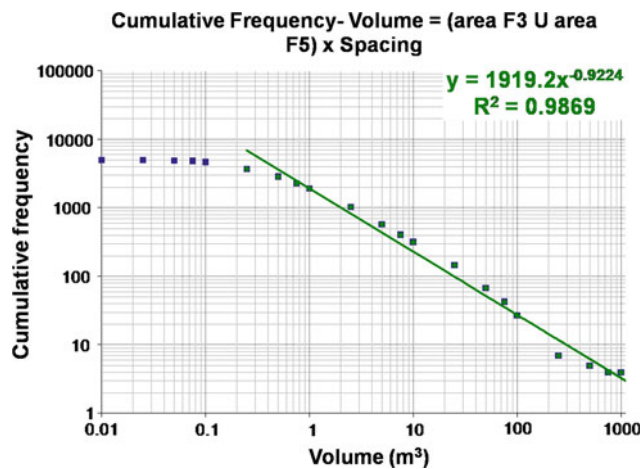


Fig. 3 Magnitude (volume in m³)—Cumulative frequency of rockfall scars, calculated from the point cloud (Santana et al. 2012)

Are There Geologic Controls of the Rockfall Volume Distribution?

The a-value in equation 2 represents the rate of rockfall activity, which unless normalized, it is also function of the size of the study area. The higher the b-value, the less important the contribution of the larger failures is, and vice versa. Compared to other published works (Dussauge et al. 2003; Guzzetti et al. 2003), the absolute b-value in Forat Negre is relatively high (Table 2). Dussauge et al. (2003), argue that rockfalls for sub-vertical cliff and for a wide range of volumes (10²–10¹⁰ m³) have b-values of 0.5 ± 0.2. The high b-value in the Andorran case could be of course attributed to the exclusion of staggered failures. However, as mentioned above no geomorphological evidences of large slope failures are found in the valley. The maximum volume with this procedure is few thousand cubic meters.

Several authors relate the b-value with the lithology and the level of fracturing of the slope (Dussauge-Peisser et al.

2002). Brunetti et al. (2009) after analyzing 19 data sets (including several rockfall data sets) concluded that variation of the scaling behavior of the non-cumulative distributions is independent of the lithological characteristics, morphological settings, triggering mechanisms, length of period and extent of the area covered by the datasets. They argue that the statistics of landslide volume is conditioned primarily by the geometrical properties of the slope or rock mass and that difference between the scaling exponents of rockfalls and landslides is consequence of the disparity of mechanisms. On the other hand, the fact that rockfalls and rock slides they studied exhibit the same frequency-volume relationship made Guzzetti et al. (2003) and Dussauge-Peisser et al. (2002) to conclude that there is no statistical difference between these types of landslides. By comparing the results of four data sets, Hungr et al. (1999) suggested that the lower exponents could correspond to areas of massive rocks with the possibility to produce a relatively greater proportion of large-magnitude structurally controlled failures.

In the case of the Forat Negre in Andorra, the structural analysis of the joint sets suggests that a geological control on the size of rockfalls may exist that could justify the greater b-value of the scar volume distribution. A field survey has been carried out of the granodiorite massif of Forat Negre aiming at determining the relative chronology of the structural features in the rock mass (Fig. 4). It was performed at key outcrops where discontinuities are better exposed. The outcrops were studied combining scanlines and detailed structural observations. It is found that set F6 was formed first as it is affected by other sets that interrupt and displace its planes. A second phase is characterized by sets F2 poorly identified with LiDAR and merged with F7. They include both very persistent conjugate faults and joints. F3 is a joint set that could be associated to this phase. It shows high scattering and undulation with amplitude up to 20 cm. The last phase is characterized by the occurrence of F1 and F4. They should be interpreted as conjugate faults that are

Table 2 Exponents of the power law fitted distributions obtained for different rockfall inventories

Reference	Location	Length of the record (year)	Range of volumes fitted (m ³)	Number of events (N)	Scaling parameter (b)
Hungur et al. (1999)	Highway 99 British Columbia	40	$10^1-8 \times 10^8$	390	-0.43
	BCR line	12	10^0-10^4	403	-0.4
	Highway 1		10^0-10^4	226	-0.7
	CP Line	22	10^0-10^4	918	-0.65
Gardner (1970) ^a	Lake Louis	Two summers	$10^{-1}-10^3$	409	-0.72
Chau et al. (2003)	Hong Kong, China			201	-0.87
Dussauge-Peisser et al. (2002)	Upper Arly, gorge French Alps		10^0-10^4	59	-0.45
	Grenoble, French Alps	60	$10^{-2}-10^6$	87	-0.41
	Yosemite, USA	77	10^0-10^5	101	-0.46
Royán et al. (2015)	Puigcercós	6.87	$10^{-2}-10^2$	3096	-0.72

^aCited in Hungur et al. (1999)

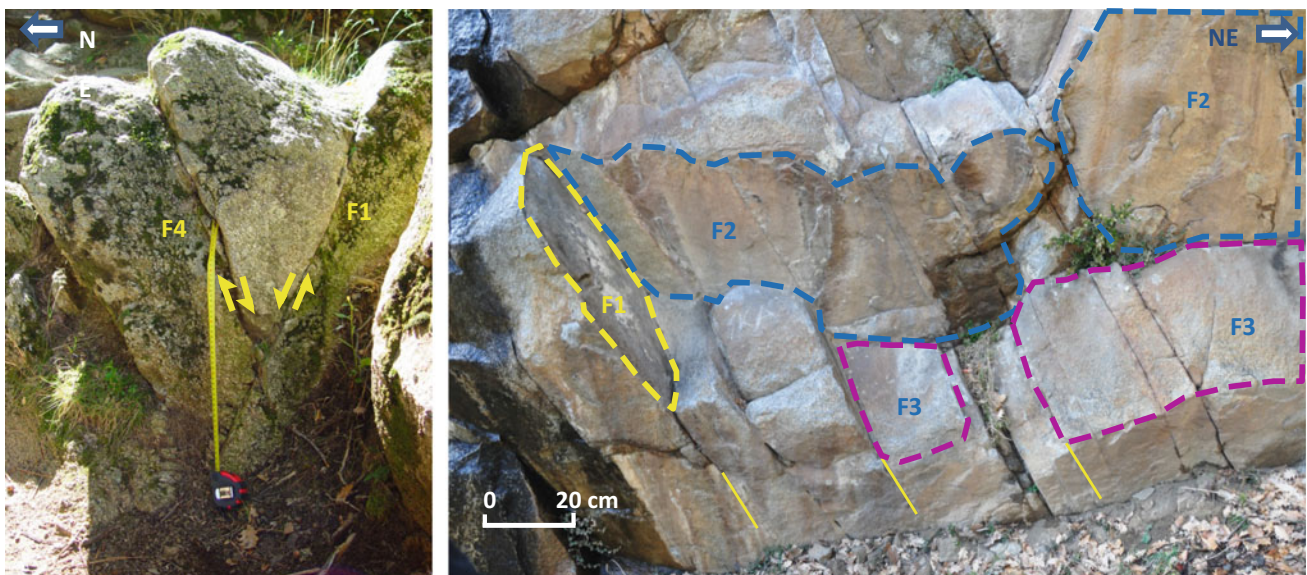


Fig. 4 (Left) Outcrop of conjugated faults F4 and F1; (right) intersection of planes of sets F1, F3 and F2

superposed and interrupt the rest of sets. F3 and F5 are joint sets usually limited and confined by fault planes of the two main deformation phases.

This survey has highlighted the frequent interruption of the basal planes (discontinuities F3 and F5) at their intersection with the tension crack and lateral release planes F7 and F1, respectively (F7 that usually plays the role of tension crack). This interruption may prevent the formation of large failures along the basal sliding surface. The analysis of the scar planes of Santana et al. (2012) has also permitted measuring the spacing of the involved discontinuity sets, as the perpendicular distances between successive planes (Mavrouli and Corominas 2017). Using the

same data, the visible length (along the dip) of the scar edges was also calculated, as the maximum edge distance along the dip of a plane (Table 3). In these table, the average length of F3 and F5 (the basal instability planes) are very similar to the average spacing of the planes of F7, although obtained by independent procedures. However, this does not always happen, the maximum measured length of F3 and F5 (27.08 and 14.65 m respectively) is much longer than the maximum spacing of F7 and one order of magnitude longer than its average spacing. This suggests that in the Forat Negre slope, the failure surface may generate by coalescence of several (although few) unfavorable dipping F3/F5 planes and/or by brittle failure

of minor rock bridges. The maximum volume will then depend on the length of the basal plane and on the resistance of the rock bridges, if any.

Assessment of the Largest Credible Volume

The assessment of the largest credible volume is crucial for the management of rockfall risk. Residential areas located below rockfall susceptible slopes have often developed strategies of risk mitigation using a combination of land use planning, stabilization and protective works (protection fences, embankments). The design of these measures and the delimitation of the hazardous areas are based on analyses for a range of expected potential rockfall volumes (Corominas et al. 2005; Abbruzzese et al. 2009; Agliardi et al. 2009; Li et al. 2009). Although some risks analyses (i.e. Hungr et al. 1999) have shown that the highest risk is associated to mid-size rockfall events ($1-10^3 \text{ m}^3$), the occurrence of rockfall events larger than the used for the design of the protective works would not be manageable and the population might be exposed at an unacceptable risk level. The question posed is what the largest credible rockfall volume can be. It is usually characterized by volumes of rock masses of several orders of magnitude greater than the events commonly observed in the study area. It must be kept in mind that the largest credible rockfall event is a reasonable largest event, not the largest conceivable event.

The analysis of the failure of a rocky slope is intrinsically linked to the knowledge of the fracture pattern of the massif which, on one side determines the volume of kinematically unstable rock mass and on the other side determines the mechanism of rupture. The instability mechanism may involve displacement along existing discontinuities either fully persistent or not and brittle failure of intact rock. It may involve single large blocks bounded by discontinuities or rock masses composed of smaller blocks. Figure 5 shows some conceptual schemes of the fracture patterns associated to the failure mechanisms. Figure 5a: simple planar failure is a rock mass affected by a fully persistent joint set. The volume mobilized is directly determined by the orientation and dip of the discontinuity and the surface topography. This

setting may generate the largest failure in the slope; Fig. 5b: if several joint sets interrupt and/or displace others, a stepped failure may develop by the coalescence of the discontinuities, which may also mobilize large rock mass volumes; Fig. 5c: In this case, a stepped failure may also develop. The failure surface of the rock mass develops across the existing joints and rock bridges. These ruptures are more difficult to define and predict due to the uncertainty associated with the persistence of the discontinuities in the rock mass. The potential for failure and the moveable volume is determined by the structure of the rock mass and the strength of the rock bridges. Volumes can be large but generally smaller than in the previous cases; Fig. 5d: failure exclusively defined by the intersection of planes of different joint sets. The interruption of the discontinuities by others results in relatively small moveable volumes.

The volumes calculated by the statistical distribution of the rockfall events are the result of the observations. The simplest way to estimate the maximal rockfall size is considering the greatest inventoried one, independently of the rock mass properties. This is feasible if the inventory used covers a long span of time (hundreds to thousands of years). Instead, Malamud et al. (2004), Picarelli et al. (2005), Brunetti et al. (2009) suggested the extrapolation of the power-law magnitude-frequency relations, for a preliminary assessment of the largest events. Malamud et al. (2004) found that the scaling factor (exponent) held for a wide range of sizes (from 10^{-3} to 10^6 m^3). The question that arises is whether this can lead to an overestimation of volumes and an oversizing of the solutions. For the detachment of large rock masses the local characteristics of the jointed rock mass such as continuity lengths of the discontinuity sets and spacings are relevant. These characteristics might be a possible reason for the truncation of the afore-mentioned distributions, as the found in some rockfall records. Brunetti et al. (2009) found that some landslide data sets exhibit a deviation of the power-law fitted tail, for large landslides. They suggested that this deviation may be the result of undersampling or due to geometrical constraints such as that a landslide cannot be larger than the slope where the failure occurs (Guzzetti et al. 2002b). In fact, deviations are observed at both high and low magnitudes (Stark and

Table 3 Measured areas, lengths and spacings of the discontinuity sets (Mavrouli and Corominas 2017)

Discontinuity	F1	F3	F5	F7
Max spacing (m)	8.09	6.35	4.11	5.60
Average spacing (m)	2.11	1.84	0.76	1.22
Median spacing (m)	1.63	1.22	0.53	1.00
Max area (m^2)	121	236	144	213
Max length (m)	19.85	27.08	14.65	19.14
Average length (m)	0.96	1.19	0.99	1.45
Median length (m)	0.76	1.04	0.73	0.89

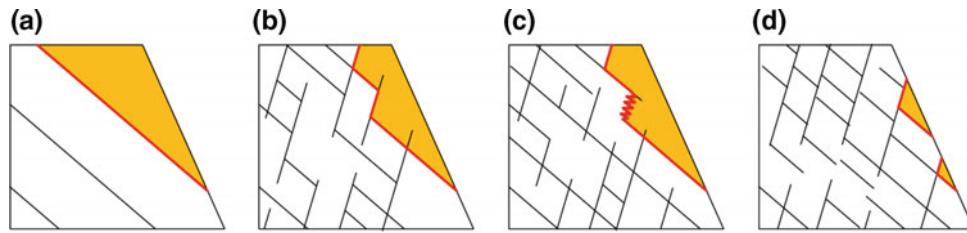


Fig. 5 Conceptual scheme of fracture pattern and development of a rock mass failure. Notice that the size of the moveable mass diminishes from a to d

Hovius 2001; Brardinoni and Church 2004; Guthrie and Evans 2004).

The assessment of the maximum possible rockfall volume at a rock slope presents several uncertainties. The unstable volumes are not always visible on the surface and additional information is required about both the orientation, spacing and persistence of discontinuities in the rock mass, which is rarely available (Palmström 2001; Elmouttie and Poropat 2012; Lambert et al. 2012; Wyllie and Mah 2004). These are critical factors for the determination of failure mechanisms too. Instability is much more likely to occur if spacings are dense and joints are fully persistent, given the usually much higher resistance of intact rock compared to that of joints (Einstein et al. 1983). The above procedures are usually applied in the detection of sizes commonly observed detachment, but do not include extreme events that could be produced in particularly adverse conditions. Setting a realistic maximum volume of detachment is still a challenge.

The role of the cliff morphology and structure on the rockfall detachment has been highlighted by Frayssines and Hantz (2006). Rosser et al. (2007) suggested that small rockfall detachments may accentuate unstable morphological features such as rock spurs and overhangs. These features may become the source of larger failures in the area and the small rockfall events could appear in this locations as precursors of the failure. In fact sustained rockfall activity for tens of years was observed before the occurrence of rock avalanches in Mount Fletcher in New Zealand (McSaveney 2002). The assessment of the maximum credible rockfall volume in the Forat Negre, that could not be identified by the analysis of the rockfall scars, is presented here summarizing the work of Mavrouli et al. (2015) and Mavrouli and Corominas (2017). The cinematically detachable rock masses are identified using a digital elevation model (DEM) and applying the Markland criterion (Hoek and Bray 1981) in each cell in the DEM where the outcrop of unfavorable discontinuities is assumed. The size of the unstable areas are defined by the addition of all the adjacent cells that meet the criteria of Markland. The distribution of potentially unstable volumes are calculated based on the areas of unstable cells in the DEM which are subsequently transformed into equivalent volumes (Fig. 6).

This analysis describes a conservative scenario with the following assumptions: (i) the whole of the unstable mass is separated at a time, regardless the possible occurrence of successive failures; (ii) all representative joint sets of the rock mass are present in each cell of the slope and (iii) for calculating the volume is considered that discontinuities outcrop in the lowest part of the unstable cells. No restriction by lateral confinement is imposed for the detachment of the rock mass. The procedure has been applied in the sector Forat Negre at the Solà de Santa Coloma, Andorra and implemented in a GIS.

The sectors containing rock volumes kinematically movable were overlapped to orthophotos in order to verify instability and to delineate smaller masses within the larger ones.

The areas of these sectors are indicative of the size of the rockfalls that can occur in this slope. In order to convert the area A , in volume V , two simple shapes and alternative rock masses mobilized are assumed: cubic or prismatic. For both, the base corresponds to the area A . The height depends on the persistence of basal plane within the rock mass (see joint length in Fig. 6). In the cubic form this length is taken as $L = \sqrt{A}$ and prismatic as $L = 0.5\sqrt{A}$. The cubic and prismatic volumes are calculated respectively by Eqs. (4) and (5).

$$V = A^{3/2} \quad (4)$$

$$V = 0.5A^{3/2} \quad (5)$$

The maximum volumes obtained by this analysis are 50,000–25,000 m³ for cubic and prismatic volumes respectively (Fig. 7). The largest basal area obtained is 1361 m². The tails of the volume distributions obtained are fitted to negative power laws whose b-values are -0.57 and -0.55 , respectively. As the concurrence of all the above mentioned hypotheses (i) to (iii) is highly unlikely and the assumptions conservative, these volumes set an upper limit for rockfalls in the study area.

The size distribution of scars observed (see Fig. 3) is an empirical evidence of rockfalls that occurred in the past. Instead, the kinematically movable rock masses indicate

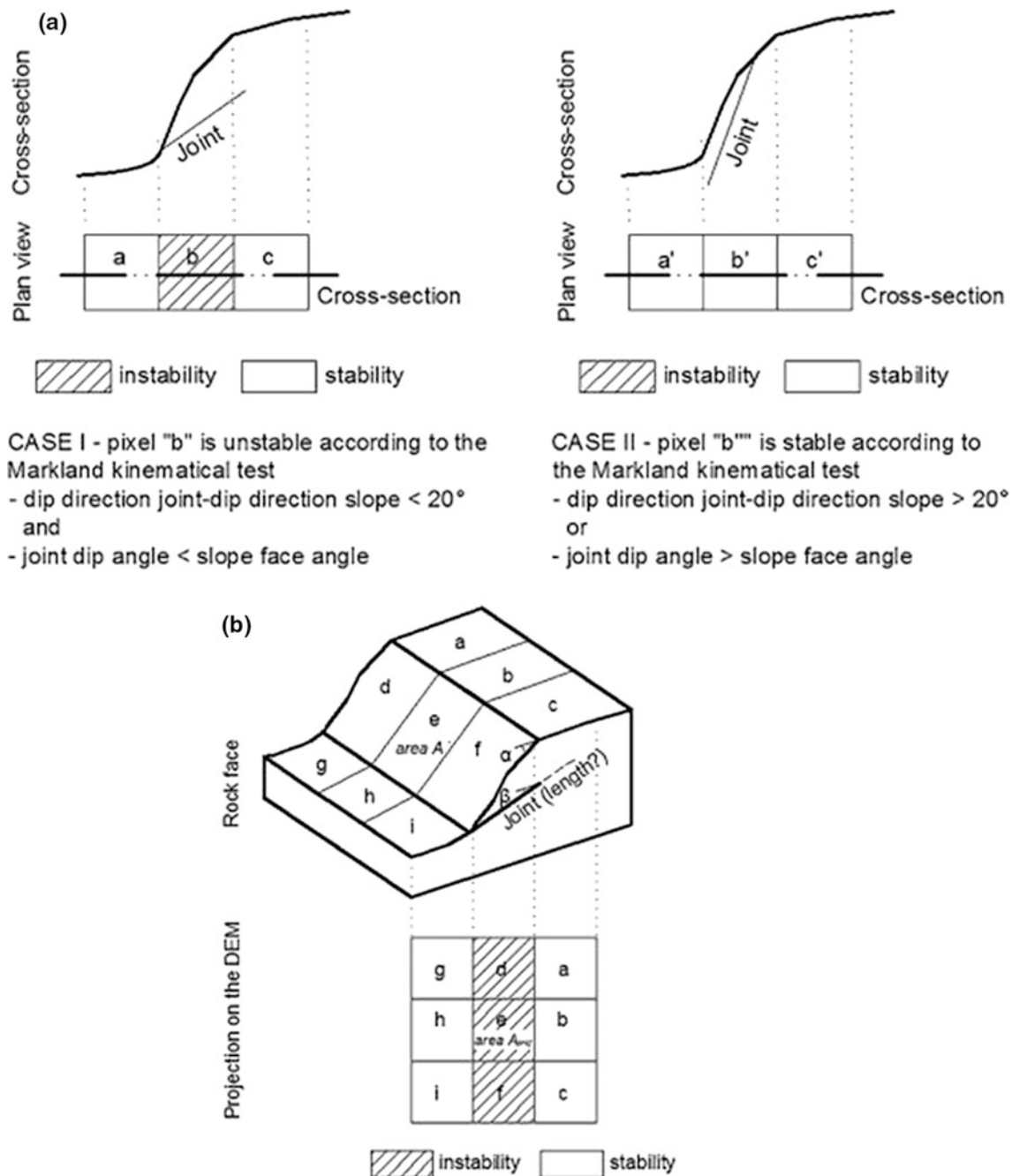


Fig. 6 Detection cinematically movable rock volumes in a DEM. *Left a* stability test for the cell and *b* formation of unstable volumes by aggregation kinematically unstable adjacent cells (modified from Mavrouli et al. 2015)

hypothetical rockfalls that could occur in the future. Comparing the two distributions, the difference between the maximum volumes of scars (about 3000 m^3) and the kinematically movable masses of rock ($25,000$ or $50,000 \text{ m}^3$) is one order of magnitude. This difference is mainly attributable to the divergence of the assumptions made. Calculating volumes scars it is based on the dimensions of the basal planes of unstable joints, which is the part of the

discontinuity in the slope that remains exposed after rupture. Conversely, on detecting the mass of kinematically movable rock, discontinuities are considered persistent and it is assumed that F3 and F5 joint sets outcrop in each cell of the DEM. Therefore, the extent of the surface of discontinuity which is involved in the detachment is greater. It is worth noticing that the kinematically movable rock masses generate continuous basal planes up to 1361 m^2 . However, these

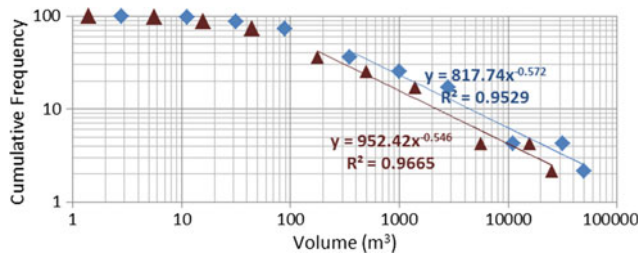


Fig. 7 Distribution (cumulative frequency) of largest potential rockfall volumes for cubic forms (*diamond*) and prismatic (*triangles*) shapes (Mavrouli et al. 2015)

planes are not observed on the actual slope, where the maximum detected area is 213 m² (Mavrouli and Corominas 2017) and in any case, the largest potential kinematically detachable volume calculated is less than 10⁵ m³.

Defining Credible Risk Scenarios

In terms of rockfall hazard assessment, answering to the question on whether the MF relations can be used to predict the probability of occurrence of large events (rock slides, rock avalanches), larger than those inventoried, is not a trivial issue. As mentioned before, the occurrence of events larger than the observed in historical and/or prehistorical records can be unmanageable and may pose a risk considered socially unacceptable. Powerful analytical and numerical tools are nowadays available and despite the uncertainties in relation to the fracture pattern and the properties of the joints and rock mass several, they can be used to analyze critical slopes. However, their use for regional (or spatially distributed) analysis is still in its infancy.

Various reasons may be accounted for checking the validity of the extrapolation of the MF for the prediction of large slope failures in contexts such as in the case of Andorra. Large massive rock slope failures (large rock mass falls, large rockslides or rock avalanches) have not been identified in the area. The occurrence of large rockslides and rock avalanches has geomorphic consequences which can be deciphered by means of the analysis of the landscape (Fig. 8). The detachment of large rock volumes from the source area can be often identified by the presence of large prominent scarps or arcuate depressions on the rock wall as well as by the long-runout accumulation of debris (Soeters and Van Westen 1996; Hewitt 2002; Ballantyne and Stone 2004).

On the other hand, the distribution of large slope failures in mountain ranges does not look like random. Large landslides are found in sectors of mountain fronts representing distinct topographic, geomorphic, and geologic characteristics that either individually or in combination favors mountain front collapse (Hermanns and Strecker 1999; Jarman et al. 2014). Large size rockslides and rock avalanches are often associated to unfavorable geostructural settings and a variety of geometries have been identified as having a potential for catastrophic failure (Hutchinson 1988). The role of both the strength and structure of the rock mass has been intensively discussed by Fell et al. (2007) and Glastonbury and Fell (2010) and found that single or two persistent intersecting discontinuities (bedding planes, schistosity, faults, stress release joints) are systematically involved in occurrence of rapid rockslides. Similar structural controls have been found elsewhere (i.e. Hermanns and Strecker 1999; Hungr and Evans 2004; Brideau et al. 2009).

A recent study of large-scale rock slope failures in the Eastern Pyrenees (including the Principality of Andorra) using imagery and field surveys (Jarman et al. 2014), has



Fig. 8 Two granodiorite rock mass outcrops in the Pyrenees, showing different pattern of instability. *Yellow dashed lines* define large sliding surfaces. (*Left*) Pala de Morrano, Aigüestortes-Sant Maurici National Park, Central Pyrenees. Exposed basal sliding planes (030°/52°) either

single or step-path may generate surfaces over 4000 m²; (*Right*) Forat Negre-Borrassica in the Solà de Santa Coloma, Principality of Andorra, Eastern Pyrenees. The largest basal sliding plane (155°/57°) measured has an area of 213 m²

identified 30 main large slope failures and further 20 smaller or uncertain cases. This inventory shows no obvious regional pattern or clustering and a surprisingly sparse population that affects 45–60 km² or 1.5–2.0% of the 3000 km² glaciated core of the mountain range, with others in fluvial valleys just beyond. From them, only 27% can be considered as large catastrophic events (rock or debris avalanches) and none of them in the Valira river valley where the slope of Forat Negre is located. For comparison, in the Alps, 5.6% of the entire 6200 km² montane area is affected by deep-seated gravitational slope deformations alone (Crosta et al. 2013) and up to 11% in the Upper Rhone basin (Pedrazzini et al. 2016). This sparsity has been interpreted by a low-intensity glaciation and less subsequent debutching, relative tectonic stability and small fluvial incision (Jarman et al. 2014). In the case of Forat Negre, this type of large failure has not occurred during the last thousands of years and should not be considered as a credible scenario.

Fragmentation in Rockfalls

It is assumed that the detached mass may break up on impact (Cruden and Varnes 1996; Hungr et al. 2014), however little attention has been paid to rockfall fragmentation. Rockfalls may involve a rock mass including discontinuities, which usually disintegrates along the path. The rockfall fragmentation is the process by which the detached mass loses its integrity while falling from a steep slope and breaks up into smaller pieces. Normally, this occurs during the first impacts on the ground (Wang and Tonon 2010). The fragmentation (Figs. 9 and 10) may consist of the separation of the rock blocks existing in the detached rock mass bounded by discontinuities (disaggregation), the breakage of the rock blocks during the impacts, or both (Ruiz-Carulla et al. 2015b).

Fragmentation invariably leads to a reduction of the particle size. The importance of the rockfall fragmentation in risk analysis has been discussed by Corominas et al. (2012). The definition of the initial volume of the rockfalls is a basic input parameter for trajectographic analysis. Rock breakage reduce the kinetic energy of the individual particles. Analyses performed with the volume of a non-fragmented rock mass produce results significantly different from the obtained if the resultant rock fragments are used instead (Okura et al. 2000; Dorren 2003). Working with the initial volume of a non-fragmented rock mass leads to the over-estimation of the kinetic energy and the reach. Large blocks follow straight paths and display farther stopping points than the small ones. These effects may change significantly the way rockfalls interact with the terrain and affect the probability of impact on exposed elements, their vulnerability and the design of the protective elements (Volkwein et al. 2011).



Fig. 9 Block fragmentation by breakage in a real scale test in Vallirana (Barcelona, Spain)



Fig. 10 Rock fall fragmentation by the disaggregation of the original rock mass in Estany Gento, Central Pyrenees, Spain. Most of the block faces are joint planes present in the in situ rock mass. Notice that crushing of the fragments is virtually absent

Furthermore, if fragmentation is not accounted, the frequency and probability of impact is underestimated. The

original rock mass is divided into a large number of fragments, which leads to multiply the probability of impact by a factor “*n*” equal to the number of new blocks generated (Corominas et al. 2012).

Currently available simulation programs for modelling the trajectory of the rockfalls (i.e. Jones et al. 2000; Dorren et al. 2006; Bourrier et al. 2009) allow calculating the distance travelled, height of jump, the kinetic energy at different points of the path and make a zonation of the exposed area. The major limitation of most of these programs is that they assume that any rock mass detached from a wall or cliff, regardless of the volume, arrives intact at the arresting point, which is not real. Some codes incorporate a fragmentation module for propagation analysis such as HY-STONE (Guzzetti et al. 2002a; Agliardi and Crosta 2003) which includes a trained neural network. The model is efficient for predicting whether a block of rock breaks or not but it may have difficulties in defining the number and size of fragments observed in reality. Salciarini et al. (2009) used a model of discrete elements to simulate the effects of fragmentation using software UDEC, and simulation results indicate that both the position of the blocks and the extent of the accumulation zone are strongly affected by fragmentation process of the rock mass.

Fragmentation in rockfalls is a complex physical mechanism, still little known and difficult to simulate (Chau et al. 2002; Zhang et al. 2000). The analysis of fragmentation is performed by measuring the size of the resultant fragments. This can be done either manually or by means of image analysis (Crosta et al. 2007; Locat et al. 2006). The degree of fragmentation may be calculated by the comparison of parameters representing the size distribution of the fragments before and after the fragmentation, such as the *d*50 diameter or the mean size. This approach is used in mining industry to assess the efficiency of blasting and it can be associated to the explosive energy and powder factors (Kuznetsov 1973). Similarly, Locat et al. (2006) determined the degree of fragmentation for rock avalanches, by comparing the mean diameters of the blocks within the intact rock mass and the deposited fragments.

If data are available, both the block size distribution of the in situ rock mass (IBSD) and that of the entire fragmented deposit can be used (Latham and Lu 1999). The block size distribution is typically represented as a grain size curve, in terms of percentage of material passing a certain size, typically with 3 or 4 orders of magnitude. Several researchers have found that the BSD of the fragments follows a power law (Turcotte 1986; Poulton et al. 1990; Locat et al. 2006; Crosta et al. 2007) with a negative exponent, whose value increases with the violence of the fragmentation process (Hartmann 1969). Fragmental rockfalls also show a similar fractal pattern. Ruiz-Carulla et al. (2016a) found that the deposits of six rockfall events yield volume distributions

of the fragments that can be fitted to power laws (Fig. 11). The rock fragments were measured directly in the field one by one with a tape. In case the deposit formed a continuous young debris cover with a high number of blocks to be measured, the methodology proposed by Ruiz-Carulla et al. (2015a) was followed. The rockfall volume involved in these events ranges from 2.6 m³ to 10,000 m³.

Despite the apparent similarity of the distributions shown in Fig. 11, they contain significant differences. The first one is the scaling factors of the tails whose values range between 0.5 and 1.3 (Table 4). The scaling factors are an expression of the intensity of the fragmentation process. This can be observed in Fig. 12, where the number of fragments generated by the breakage of each individual block is plotted against the exponents of the fitted power laws of their volume distributions. There exists a positive correlation between the number of blocks generated and the exponents of the power law. The meaning of the exponents in the case of rockfall deposits is however, less evident as it is generated from an in situ block size distribution (IBSD) of the detached mass. The fragmentation in rockfalls is a function of several variables (Dussauge et al. 2003; Wang and Tonon 2010; Hantz et al. 2014): the presence of discontinuities in the initial rock mass and their persistence, their orientation at the time of impact, the energy and angle of impact and the ground stiffness. The highest exponent of the rockfall inventoried corresponds to the case of Vilanova de Banat with a value of 1.27 and 60,000 blocks generated from a volume of 10,000 m³. It has both the largest volume and highest height of fall (Table 4). As it will be shown latter, the

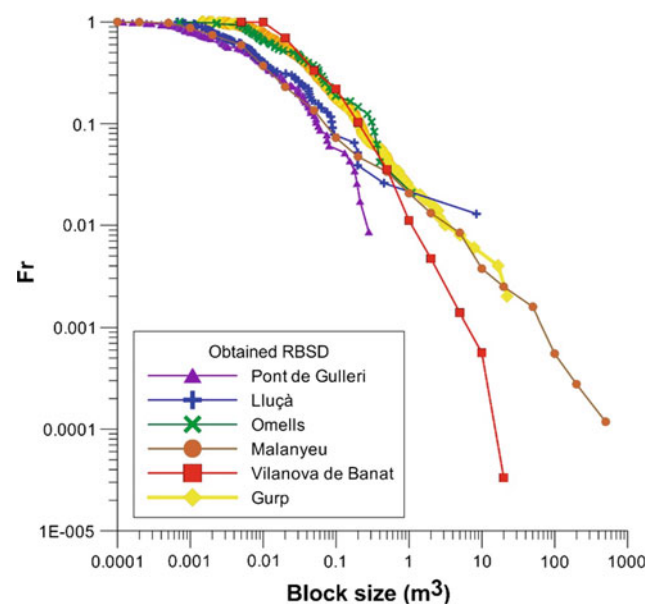


Fig. 11 Rockfall Block Size Distribution (RBSD) from 6 fragmental rockfalls events inventoried in Catalonia (from Ruiz-Carulla et al. 2017)

number of fragments generated is an order of magnitude bigger than the original IBSD. Most of the new fragments are small and appear concentrated forming a young debris cover at the base of the cliff (Ruiz-Carulla et al. 2015a). The number of fragments smaller than 0.01 m³ represents more than 60% of the total. The cases Lluçà and Omells are the opposite situation. The exponents of the fitted distribution are small (0.51–0.53) which is consistent with the small height of fall (0.6–0.8). The amount of fragments generated is partly due to the low strength of the involved rocks. The cases of Malanyeu, Gulp and Pont de Gullerí are intermediate situations with a height of fall of 10 or more meters. The higher value of the exponent in the Pont de Gullerí case is basically due to the IBSD as most of the fragments are bounded by preexisting joint faces. The rockfall block size distribution (RBSD) in this case is best fitted to an exponential law and can be considered as case of pure disaggregation.

Fractal Fragmentation Model

Most of current approaches used to obtain the RBSD consider the energy required to convert the IBSD into a new fragment-size distribution (Latham and Lu 1999; Lu and Latham 1999) and only few of them are applied to the analysis of the fragmentation of rock avalanches (Locat et al. 2006; Bowman et al. 2012; Charrière et al. 2015).

We have developed a fractal fragmentation model to characterize fragmental rockfalls (Ruiz-Carulla et al. 2015a, 2016b). The procedure aims at obtaining the rockfall block size distribution (RBSD) from the volume of the initial detached mass and its fracture pattern (IBSD) (Ruiz-Carulla et al. 2015b, 2016b). This model is based on a generic fractal fragmentation model (Perfect 1997) that considers a cubic block of unit length which is broken into small pieces according to a power law. The size distribution of the elements in a fractal system is given by (Eq. 6):

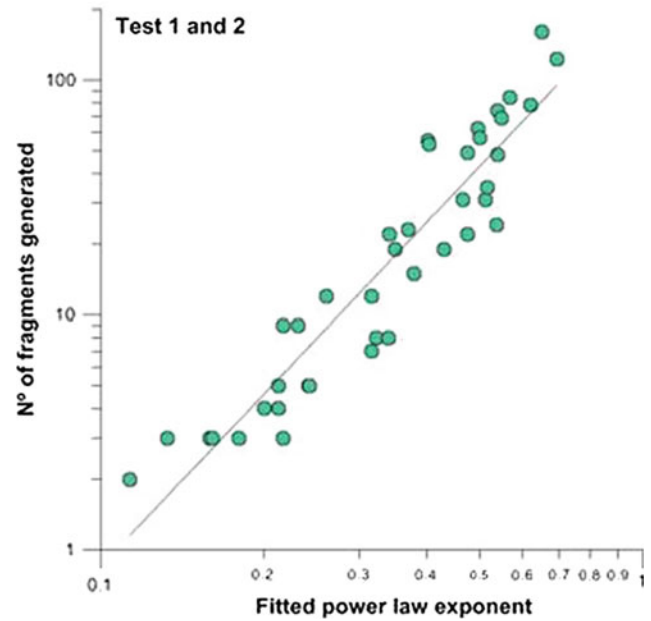


Fig. 12 Exponents of the fitted power laws of the volume distribution of the fragments generated by breakage of single blocks in real scale tests carried out in the Vallirana quarry, Spain (Ruiz-Carulla et al. 2016b)

$$N(1/b^i) = k [1/b^i]^{-D_f}; \quad i = 0, 1, 2, \dots, \infty \quad (6)$$

Where $N(1/b^i)$ is the number of elements at the level “ i ” of the hierarchy; “ k ” is the number of initiators of unit length; “ b ” is a scaling factor >1 ; and D_f is the fractal dimension of fragmentation, which can be defined as:

$$D_f = 3 + \frac{\log[P(1/b^i)]}{\log[b]} \quad (7)$$

Where $P(1/b^i)$ or P_f : It is the probability of fracture that determines the proportion of the original block that breaks and generates new fragments. P_f is physically related to the interfaces of the subunits and maximum (limit) strength. The

Table 4 Characteristics of the inventoried rockfalls (modified from Ruiz-Carulla et al. 2016b)

Joint set	Pont de Gullerí	Lluçà	Omells	Malanyeu	Vilanova de Banat	Gulp
Lithology	Schist	Sandstone	Sandstone	Limestone	Limestone	Conglomerate
Total rockfall volume (m ³)	2.6	10.7	4.2	5000	10000	100
Free fall height (m)	12	0.6	0.8	10	40	80
Max block (m ³)	0.28	8.5	1.1	445	31	22
Min. volume measured (m ³)	0.0001	0.0007	0.0007	0.0001	0.01	0.01
# of blocks measured	116	78	48	2721	1524	500
Total # of blocks calculated	116	78	48	25,500	60,000	500
Exponent of the fitted power law	0.92	0.51	0.53	0.72	1.27	0.74
Min. block size fitted (m ³)	0.001	0.001	0.01	0.001	0.01	0.01
R ² of the fitted power law	0.94	0.95	0.89	0.98	0.95	0.98

interfaces may correspond to the surfaces of existing joints, to rock anisotropy, or non-persistent joints (Perfect 1997). The range of the probability of failure is $b^{-3} < P(1/b^i) < 1$. When $P(1/b^i) = 1$ and $D_f = 3$ the whole block breaks, while for $P(1/b^i) \leq b^{-3}$ the block remains intact. The model performance is summarized in Fig. 13

The fractal fragmentation model has been adapted for the case of the rockfall. First, instead of k initial volumes of unit length, the IBSD is used as input, classifying it in bins. Second, not all the blocks of the IBSD break upon impact on the ground. To consider this, a survival rate, S_r , representing the proportion of blocks that do not break is defined.

The FFM has been applied to several cases inventoried in the Spanish Pyrenees. Here, the case of Vilanova de Banat is presented. This rockfall took place in November 2011, affecting a volume of about $10,000 \text{ m}^3$ of limestone (Ruiz-Carulla et al. 2015a). The model uses as input data the size of the rockfall (the unstable volume) and the discontinuity pattern of the detached rock mass (joint set orientations and spacing) to obtain the ISBD. A Nikon D90 digital camera with a focal length of 60 mm and 12Mp resolution was used to generate the digital surface model (DSM) of the rockfall scar. The following step was to reconstruct the volume of the detached rock mass by subtracting the DSM of the scar from the available topographic map at 1:5000 scale (before the failure). Then, the joint sets and their spacing were identified using the DSM texturized with the images and matched to the detached rock mass. Given that neither high quality photos of the source area nor a detailed digital surface model (DSM) prior to the occurrence of the rockfall were available, the volume and the IBSD obtained are subjected to a high degree of uncertainty. There is a difference between the total volume measured in the

detachment zone ($\sim 10,000 \text{ m}^3$) and the measured in the deposit (8000 m^3). However, the difference could be explained by the proportion of smaller blocks of 0.015 m^3 , which were not measured in the field.

Five joint sets using both semiautomatic and manual techniques were identified. The fracture pattern was applied to the missing rock mass volume, assuming joints of infinite persistence. Finally the IBSD is generated. We considered two different shapes for the detached mass: (a) the irregular volume reconstructed directly from the scar ($\sim 10,000 \text{ m}^3$) and (b) a prismatic shape with the same volume, to simplify the cutting tasks. In order to account for the uncertainties associated to the reconstruction of the rock mass, two volumes were used and 4 or 5 fully persistent joint sets. Figure 14 shows the pattern of both the prismatic and irregular reconstructed volumes. The IBSDs have been generated with the mentioned assumptions: prismatic and irregular; $10,000 \text{ m}^3$ volume and 5000 m^3 ; and 4 and 5 joint sets. The IBSDs obtained are shown on the right side of the figure. All tails are fitted to exponential laws with coefficients of determination close to 1.

We calibrated the model parameters in the Vilanova de Banat case study in order to obtain a RBSD that fits that observed in the field. Several combinations of the model parameters produce well fitted block volume distributions. Their values range between 0.05 and 0.34 for S_r , between 0.73 and 0.80 for P_f and between 1.6 and 3.4 for “ b ”. The χ^2 was used to optimize P_f , S_r and to check the goodness of results, obtaining a range of values between 0.02 and 0.11 for the four IBSD. Figure 15 shows the IBSD obtained from the irregular reconstructed volume, the RBSD measured in the field and RBSD obtained from the calibration of fractal fragmentation model (FFM). The results show that the RBSD can be successfully generated from the ISBDs.

It is worth noticing that fragmentation has a significant effect in the size-range between 1 and 10 m^3 . The number of blocks within this range has been reduced up to one order of magnitude. Conversely, the number of blocks smaller than 1 m^3 has increased more than one order of magnitude. This effect has direct consequences on the kinematics of the fragments with a reduction of the distances travelled, velocities. Despite of this, the survival rates (S_r) obtained indicate that up to one third of the original blocks have remained unbroken as illustrated by the 272 large scattered blocks that were measured in the field and travelled far away from the young debris cover (Ruiz-Carulla et al. 2015a).

Furthermore, the accumulated volume of the smallest blocks ($<0.01 \text{ m}^3$) has risen from an insignificant value up to more than 15% of the total. This represents an expenditure of the breakage energy that cannot be obviated.

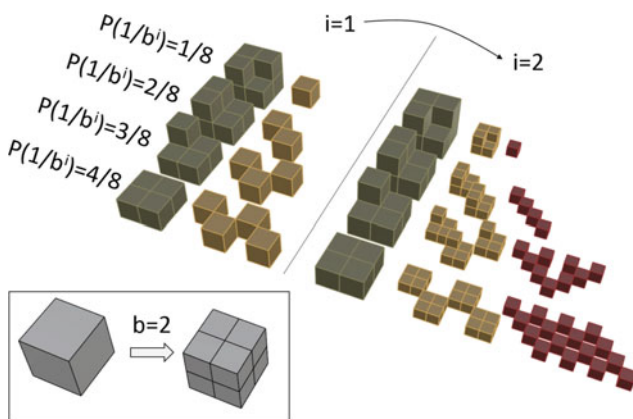


Fig. 13 Rockfall fragmentation model (Ruiz-Carulla et al. 2017)

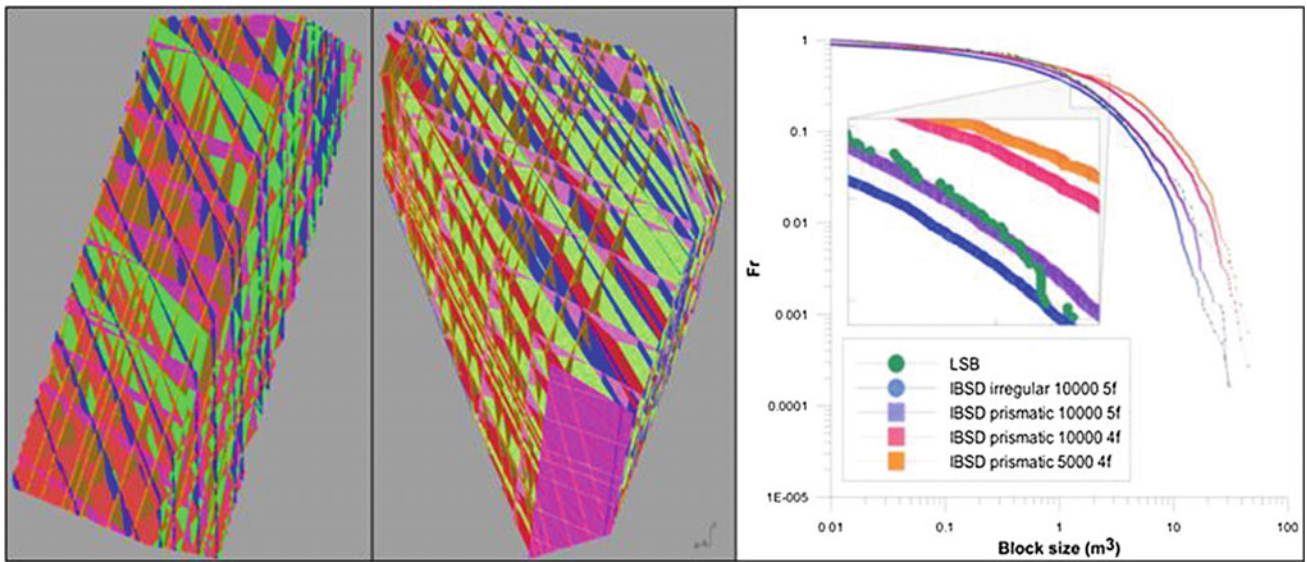


Fig. 14 Fracture model generated from the detached rock mass volume cut by the discontinuities with their actual spacings using a prismatic shape (*left*) and the reconstructed irregular shape volume of

the rockfall source (*center*). Plot of the resultant IBSD distributions considering 4 or 5 sets of fully persistent joints (*right*)

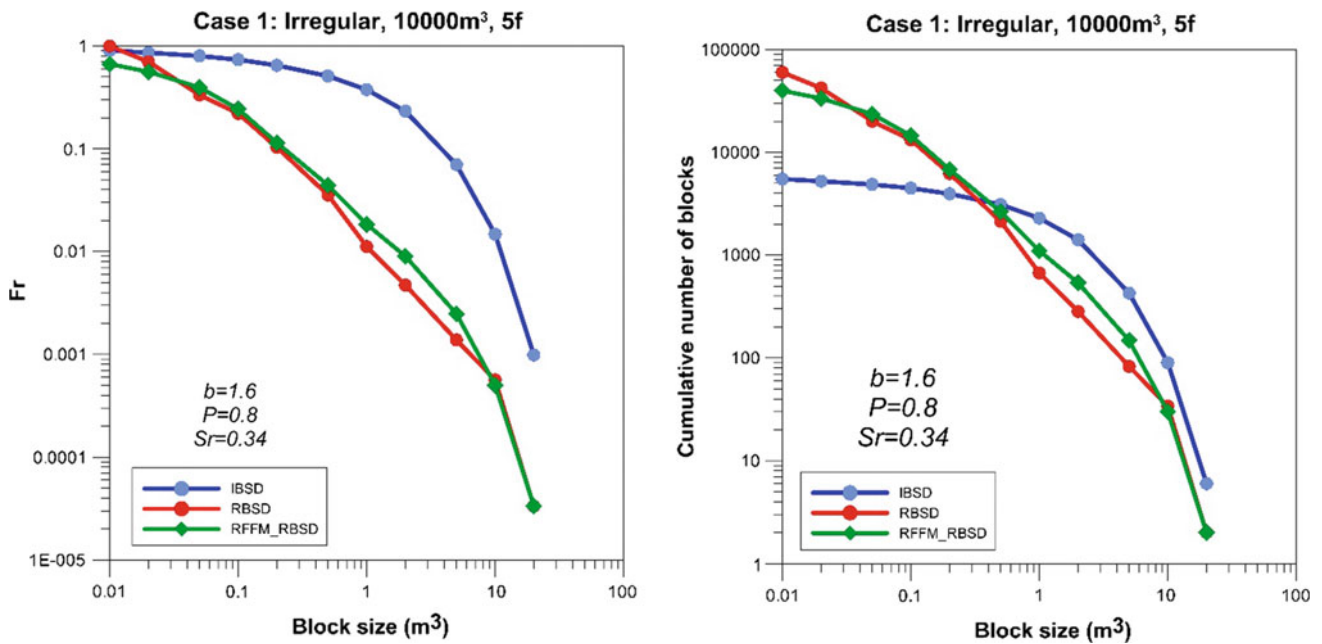


Fig. 15 The IBSD of the reconstructed volume, the observed RBD and the RBSD generated with fractal fragmentation model (RBSD—FFM) in terms of relative frequency (*left*) and cumulative number of blocks (*right*) versus block size

Further work is needed for the performance of the FFM. Several parameters are involved in the fragmentation process and the resultant RBSD such as the IBSD, the total volume detached, the impact energies and the morphology and the rigidity of the ground. The procedure in the example of Vilanova de Banat is iterative until the fit between the

observed and modeled RBSD is achieved. In order to use the FFM as predictive tool it is required the analysis of more cases to relate P_f , S_r and the scaling factor to the local geological conditions as well as to the geomechanical, and morphological characteristics of the detached rock mass and of the slope.

Final Remarks

FM relations are fundamental for performing the QRA. Most of the rockfall volume distributions are characterized by a negative power law. It has been argued that, if the statistical tests are fulfilled, they can be used to calculate the frequency of large volumes and that both rockfalls and rockslides display the same b -value. However, a critical issue is the definition of the maximum credible volume to be used in the hazard analyses and for implementing risk mitigation measures. The case of Andorra provides empirical evidence that rockfalls could be size-constrained due to the geological context as no rock avalanche deposits are found in the Valira river basin. Two analyses on the rockfall size distribution have been carried out at slope of Forat Negre. The first analysis corresponds to the observed size distribution of the rockfall scars, and it is an empirical evidence of past rockfalls. The second one calculates the kinematically detachable rock masses, indicating hypothetical rockfalls that might occur in the future. These two independent approaches differ on an order of magnitude only with a maximum credible volume between 25,000 and 50,000 m³. The volume distribution of the rockfall scars is well fitted by a power law with b -value of -0.92 , and suggests that large rockfall events are less abundant than in other mountainous regions.

The clue for such a behavior could be in the persistence of the discontinuity sets. In the slope of Forat Negre, F1 and F7 are fault sets that intersect and displace the rest of discontinuity sets as they have probably been generated during the last deformation phases in this sector of the range. They exert a control over the length of the planes of the discontinuities F3 and F5 and imply a limitation on their persistence. This volume restriction can be overcome to some extent either by coalescence of basal planes or through step-path failures involving the breakage of rock bridges. This situation however, will necessarily involve smaller volumes than in the case of fully persistent basal joints. In any case, the worst case scenarios that may be foreseen can be nowadays faced with better tools thanks to the development of the remote data collection equipment, particularly the LiDAR, digital photogrammetry and interferometric techniques. As several experiences have already shown, these techniques provide the deformation pattern and rate of movement over large terrain areas thus allowing the identification and delineation of potentially unstable masses and the implementation of EWS and evacuation strategies (i.e. Froese et al. 2009; Hermanns et al. 2013; Michoud et al. 2013).

Despite the difficulties and uncertainties associated to the generation of the IBSD and the RBSD, the results of the six rockfall events inventoried indicate that breakage of the particles is a fundamental mechanism in all-size fragmental rockfalls. The number of new generated particles increases

with the size of the rockfall and is the result of the interplay of other factors such as the strength of the rock, the height of fall and stiffness of the impact ground surface.

The FFM has successfully generated a RBSD that fits well to the observed in the field. It is able to consider both the disaggregation and breakage mechanisms of rockfalls while considering successive iterations will increase the number of small-size fragments generated. It is simple enough to be incorporated into rockfall trajectory analyses. However, its application at present is not straightforward. The model runs using the IBSD as input data and requires the definition of three additional parameters: the survival rate of the blocks present in the detached rock mass, the probability of failure that determines the proportion of each initiator block that breaks, and the scaling factor or ratio of sizes between the initial block and the fragments. In order to use this model as a predictive tool more case histories are needed to calibrate it. Finally, we argue that fragmentation cannot be obviated and must be incorporated in the rockfall hazard analyses.

Acknowledgements The authors acknowledge the support of the Spanish Economy and Competitiveness Ministry to the Rockrisk research project (BIA2013-42582-P) and of the Government of Andorra (Edicte de 10/04/2013, BOPA n°18 17/04/2014).

References

- Abbruzzese JM, Sauthier C, Labiouse V (2009) Considerations on Swiss methodologies for rock fall hazard mapping based on trajectory modelling. *Nat Hazards Earth Syst Sci* 9(4):1095–1109
- Abellan A, Vilaplana JM, Martinez J (2006) Application of a long-range terrestrial laser scanner to a detailed rockfall study at Vall de Nuria (Eastern Pyrenees, Spain). *Eng Geol* 88:136–148
- Agliardi F, Crosta GB (2003) High resolution three-dimensional numerical modelling of rockfalls. *Int J Rock Mech Min Sci* 40:455–471
- Agliardi F, Crosta GB, Frattini P (2009) Integrating rockfall risk assessment and countermeasure design by 3D modelling techniques. *Nat Hazards Earth Syst Sci* 9:1059–1073
- Amitrano D, Grasso JR, Senfaute G (2005) Seismic precursory patterns before a cliff collapse and critical point phenomena. *Geophys Res Lett* 32: L08314
- Ballantyne CK, Stone JO (2004) The Beinn Alligin rock avalanche, NW Scotland: cosmogenic ¹⁰Be dating, interpretation and significance. *Holocene* 14:448–453
- Bourrier F, Dorren L, Nicot F, Berger F, Darve F (2009) Toward objective rockfall trajectory simulation using a stochastic impact model. *Geomorphology* 110(3):68–79
- Bourrier F, Dorren L, Hungr O (2013) The use of ballistic trajectory and granular flow models in predicting rockfall propagation. *Earth Surf Proc Land* 38:435–440
- Bowman ET, Take AW, Rait KL, Hann C (2012) Physical models of rock avalanche spreading behaviour with dynamic fragmentation. *Can Geotech J* 49:460–476
- Brardinoni F, Church M (2004) Representing the landslide magnitude-frequency relation: Capilano river basin, British Columbia. *Earth Surf Proc Land* 29:115–124

- Brideau MA, Yan M, Stead D (2009) The role of tectonic damage and brittle rock fracture in the development of large rock slope failures. *Geomorphology* 103:30–49
- Brunetti MT, Guzzetti F, Rossi M (2009) Probability distributions of landslide volumes. *Nonlin Processes Geophys* 16:179–188
- Budetta P (2004) Assessment of rockfall risk along roads. *Nat Hazards Earth Syst Sci* 4:71–81
- Charrière M, Humair F, Froese C, Jaboyedoff M, Pedrazzini A, Longchamp C (2015) From the source area to the deposit: collapse, fragmentation, and propagation of the Frank Slide. *Geol Soc Am Bull* 128:332–351
- Chau KT, Wong RHC, Wub JJ (2002) Coefficient of restitution and rotational motions of rockfall impacts. *Int J Rock Mech Min Sci* 39:69–77
- Chau KT, Wong RCH, Liu J, Lee CF (2003) Rockfall hazard analysis for Hong Kong based on rockfall inventory. *Rock Mech Rock Eng* 36:383–408
- Copons R (2007) Avaluació de la perillositat de caigudes de blocs rocosos al Solà d'Andorra la Vella. *Monografies del CENMA*
- Copons R, Vilaplana JM, Corominas J, Altimir J, Amigó J (2004) Rockfall risk management in high-density urban areas. The Andorran experience. In: Glade T, Anderson M, Crozier MJ (eds) *Landslide hazard and risk*. Wiley, Chichester, pp 675–698
- Corominas J, Mavrouli O (2011) Rockfall quantitative risk assessment. In: Lambert S, Nicot F (eds) *Rockfall engineering*. ISTE Ltd. & Wiley, pp 255–301
- Corominas J, Moya J (2008) A review of assessing landslide frequency for hazard zoning purposes. *Eng Geol* 102:193–213
- Corominas J, Copons R, Moya J, Vilaplana JM, Altimir J, Amigó J (2005) Quantitative assessment of the residual risk in a rock fall protected area. *Landslides* 2:343–357
- Corominas J, Mavrouli O, Santana D, Moya J (2012) Simplified approach for obtaining the block volume distribution of fragmental rockfalls. In: Eberhardt E et al (eds) *Proceedings of the 11 International Symposium on Landslides, Banff, Canada, vol 2*. CRC Press/Balkema, Leiden, pp 1159–1164
- Corominas J, van Westen C, Frattini P, Cascini L, Malet JP, Fotopoulou S, Catani F, Van Den Eeckhaut M, Mavrouli O, Agliardi F, Pitilakis K, Winter MG, Pastor M, Ferlisi S, Tofani V, Hervás J, Smith JT (2014) Recommendations for the quantitative analysis of landslide risk. *Bull Eng Geol Environ* 73:209–263
- Crosta GB, Agliardi F (2003) Failure forecast for large rock slides by surface displacement measurements. *Can Geotech J* 40:176–191
- Crosta GB, Frattini P, Fusi F (2007) Fragmentation in the Val Pola rock avalanche, Italian Alps. *J Geophys Res* 112:F01006
- Crosta GB, Frattini P, Agliardi F (2013) Deep seated gravitational slope deformations in the European Alps. *Tectonophysics* 605:13–33
- Cruden DM, Varnes DJ (1996) *Landslide types and processes*. In: Turner AK, Schuster RL (eds) *Landslides investigation and mitigation*. National Research Council, Transportation Research Board, Special Report 247, pp 36–75
- Davies TR, McSaveney MJ (2002) Dynamic simulation of the motion of fragmenting rock avalanches. *Can Geotech J* 39:789–798
- Davies TR, McSaveney MJ, Hodgson KA (2009) A fragmentation–spreading model for long-runout rock avalanches. *Can J Geotech* 36:1096–1110
- Dorren LKA (2003) A review of rockfall mechanics and modeling approaches. *Prog Phys Geogr* 27(1):69–87
- Dorren L, Berger F, Putters US (2006) Real size experiments and 3D simulation of rockfall on forested and nonforested slopes. *Nat Hazards Earth Syst Sci* 6:145–153
- Dussauge C, Grasso JR, Helmstetter A (2003) Statistical analysis of rockfall volume distributions: implications for rockfall dynamics. *J Geophys Res* B6(108):2286
- Dussauge-Peisser A, Helmstetter A, Grasso JR, Hanz D, Desvarreux P, Jeannin M, Giraud A (2002) Probabilistic approach to rockfall hazard assessment: potential of historical data analysis. *Nat Hazards Earth Syst Sci* 2:15–26
- Eberhardt E (2008) The role of advanced numerical methods and geotechnical field measurements in understanding complex deep-seated rock slope failure mechanisms. *Can Geotech J* 45:484–510
- Eberhardt E, Stead D, Coggan JS (2004) Numerical analysis of initiation and progressive failure in natural rock slopes—the 1991 Randa rockslide. *Int J Rock Mech Min Sci* 41:69–87
- Einstein HH, Veneziano D, Baecher GB, O'Reilly KJ (1983) The effect of discontinuity persistence on rock slope stability. *Int J Rock Mech Min Sci Geomech Abstracts* 20:227–236
- Elmouttie MK, Poropat GV (2012) A method to estimate in situ block size distribution. *Rock Mech Rock Eng* 45(3):401–407
- El-Ramly H, Morgenstern NR, Cruden DM (2002) Probabilistic slope stability analysis for practice. *Can Geotech J* 39:665–683
- Evans S, Hungr O (1993) The assessment of rockfall hazard at the base of talus slopes. *Can Geotech J* 30:620–636
- Fell R, Ho KKS, Lacasse S, Leroi E (2005) A framework for landslide risk assessment and management. In: Hungr O, Fell R, Couture R, Eberhardt E (eds) *Landslide risk management*. Taylor and Francis, London, pp 3–25
- Fell R, Glastonbury J, Hunter G (2007) Rapid landslides: the importance of understanding mechanisms and rupture surface mechanisms. *Q J Eng Geol* 40:9–27
- Ferlisi S, Cascini L, Corominas J, Fabio M (2012) Rockfall risk assessment to persons travelling in vehicles along a road: the case study of the Amalfi coastal road (southern Italy). *Nat Hazards* 62:691–721
- Ferrero AM, Migliazza M, Roncella R, Rabbi E (2011) Rock slopes risk assessment based on advanced geotechnical survey techniques. *Landslides* 8(2):221–231
- Frayssines M, Hantz D (2006) Failure mechanisms and triggering factors in calcareous cliffs of the Subalpine Ranges (French Alps). *Eng Geol* 86(4):256–270
- Froese CR, Moreno F, Jaboyedoff M, Cruden DM (2009) 25 years of movement monitoring of South Peak, Turtle Mountain: understanding the hazard. *Can Geotech J* 46:256–269
- Fukuzono T (1990) Recent studies on time prediction of slope failure. *Landslide News* 4:9–12
- Gischig V, Loew S, Kos A, Raetzo H, Lemy F (2009) Identification of active release planes using ground-based differential InSAR at the Randa rock slope instability, Switzerland. *Nat Hazards Earth Syst Sci* 9:2027–2038
- Glastonbury J, Fell R (2010) Geotechnical characteristics of large rapid rock slides. *Can Geotech J* 47:116–132
- Guthrie RH, Evans SG (2004) Analysis of landslide frequencies and characteristics in a natural system, coastal British Columbia. *Earth Surf Proc Land* 29:1321–1339
- Guzzetti F, Crosta G, Detti R, Agliardi F (2002a) STONE: a computer program for the three-dimensional simulation of rock-falls. *Comput Geosci* 28:1079–1093
- Guzzetti F, Malamud BD, Turcotte DL, Reichenbach P (2002b) Power-law correlations of landslide areas in Central Italy. *Earth Planet Sci Lett* 195:169–183
- Guzzetti F, Reichenbach P, Wieczorek GF (2003) Rockfall hazard and risk assessment in the Yosemite Valley, California, USA. *Nat Hazards Earth Syst Sci* 3:491–503
- Haneberg WC (2008) Using close range terrestrial digital photogrammetry for 3-D rock slope modeling and discontinuity mapping in the United States. *Bull Eng Geol Environ* 67:457–469

- Hantz D, Vengeon JM, Dussauge-Peisser C (2003) An historical, geomechanical and probabilistic approach to rock-fall hazard assessment. *Nat Hazards Earth Syst Sci* 3(6):693–701
- Hantz D, Rossetti JP, Servant F, D'Amato J (2014) Etude de la distribution des blocs dans un éboulement pour l'évaluation de l'aléa. *Proceedings of Rock Slope Stability 2014, Marrakesh*, p 10
- Hartmann WK (1969) Terrestrial, lunar and interplanetary rock fragmentation. *Icarus* 10:201–213
- Heritage GL, Large ARG (2009) *Laser scanning for the environmental sciences*. Wiley-Blackwell, London, 288 p. ISBN 978-1-4051-5717-9
- Hermanns R, Strecker MR (1999) Structural and lithological controls on large Quaternary rock avalanches (sturzstroms) in arid north-western Argentina. *Geol Soc Am Bull* 111:934–948
- Hermanns R, Blikra LH, Anda E, Saintot A, Dahle H, Oppikofer T, Fischer L, Bunkholt H, Böhme M, Dels JF, Lauknes TR, Redfield TF, Osmundt T, Eiken T (2013) Systematic mapping of large unstable rock slopes in Norway. In: Margottini C et al (eds) *Landslide science and practice*, vol 1. Springer, Berlin, pp 29–34. doi:10.1007/978-3-642-31325-7_3
- Hewitt K (1999) Quaternary moraines vs. catastrophic rock avalanches in the Karakoram Himalaya, Northern Pakistan. *Quat Res* 51:220–237
- Hewitt K (2002) Styles of rock avalanche depositional complexes conditioned by very rugged terrain, Karakoram Himalaya, Pakistan. In: Evans SG and DeGraff IV *Catastrophic landslides: effects, occurrence, and mechanisms*, *Reviews in Engineering Geology* 15, 345–377
- Hewitt K, Clague JJ, Orwin JF (2008) Legacies of catastrophic rock slope failures in mountain landscapes. *Earth Sci Rev* 87:1–38
- Hoek E, Bray JW (1981) *Rock slope engineering*, Institution of Mining and Metallurgy, London
- Hovius N, Stark CP, Allen PA (1997) Sediment flux from a mountain belt derived by landslide mapping. *Geology* 25:231–234
- Hsü KJ (1978) Albert Heim: observations of landslides and relevance to modern interpretations. In: Voight B (ed) *Rockslides and avalanches: 1, Natural phenomena*. Elsevier, Amsterdam, pp 70–93
- Hungr O (2016) A review of landslide hazard and risk methodology. In: Aversa S, Cascini L, Picarelli L, Scavia C (eds) *Landslides and engineered slopes: experience, theory and practice*, vol 1. CRC press, pp 3–27. ISBN 978-1-138-02989-7
- Hungr O, Evans SG (2004) The occurrence and classification of massive rock slope failure. *Felsbau* 22:1–12
- Hungr O, Evans SG, Hazzard J (1999) Magnitude and frequency of rock falls and rock slides along the main transportation corridors of southwestern British Columbia. *Can Geotech J* 36:224–238
- Hungr O, Corominas J, Eberhardt E (2005) Estimating landslide motion mechanisms, travel distance and velocity. In: Hungr O, Fell R, Couture R, Eberhardt E (eds) *Landslide risk management*. Taylor and Francis, London, pp 99–128. ISBN 041538043X
- Hungr O, McDougall S, Wise M, Cullen M (2008) Magnitude–frequency relationships of debris flows and debris avalanches in relation to slope relief. *Geomorphology* 96:355–365
- Hungr O, Leroueil S, Picarelli L (2014) The Varnes classification of landslides types, an update. *Landslides* 11:167–194
- Hutchinson JN (1988) Morphological and geotechnical parameters of landslides in relation to geology and hydrogeology. In: Bonnard C (ed) *Landslides*. *Proceedings of the 5th International Conference on Landslides*, vol 1. Lausanne, pp 3–35
- Jaboyedoff M, Metzger R, Oppikofer T, Couture R, Derron MH, Locat J, Turmel D (2007) New insight techniques to analyze rock-slope relief using DEM and 3D-imaging cloud points: COLTOP-3D software. In: Eberhardt E, Stead D, Morrison T (eds) *Rock mechanics: meeting society's challenges and demands*, vol 1. Taylor & Francis, pp 61–68
- Jaboyedoff M, Couture R, Locat P (2009) Structural analysis of Turtle Mountain (Alberta) using digital elevation model: toward a progressive failure. *Geomorphology* 103:5–16
- Jaboyedoff M, Oppikofer T, Abellán A, Derron MH, Loye A, Metzger R, Pedrazzini A (2012) Use of LIDAR in landslide investigations: a review. *Nat Hazards* 61:5–28
- Jarman D, Calvet M, Corominas J, Delmas M, Gunnell Y (2014) Large-scale rock slope failures in the eastern Pyrenees: identifying a sparse but significant population in paraglacial and parafluvial contexts. *Geogr Ann A* 96(3):357–391
- Jones CL, Higgins JD, Andrew RD (2000) Colorado rockfall simulation program, version 4.0. Colorado Geological Survey. <http://www.geosurvey.state.co.us>
- Kemeny J, Post R (2003) Estimating three-dimensional rock discontinuity orientation from digital images of fracture traces. *Comput Geosci* 29(1):65–77
- Kemeny J, Norton B, Turner K (2006) Rock slope stability analysis utilizing ground-based LiDAR and digital image processing. *Felsbau* 24:8–16
- Kromer RA, Hutchinson DJ, Latto MJ, Gauthier D, Edwards T (2015) Identifying rock slope failure precursors using LiDAR for transportation corridor hazard management. *Eng Geol* 195:93–103
- Kuznetsov VM (1973) The mean diameter of fragments formed by blasting rock. *J Min Sci* 9:144–148
- Lambert C, Thoeni K, Giacomini A, Casagrande D, Sloan S (2012) Rockfall hazard analysis from discrete fracture network modelling with finite persistence discontinuities. *Rock Mech Rock Eng* 45(5):871–884
- Latham J, Lu P (1999) Development of an assessment system for the blastability of rock masses. *Int J Rock Mech Min Sci* 36:41–55
- Lato M, Diederichs MS, Hutchinson J, Harrap R (2009) Optimization of LiDAR scanning and processing for automated structural evaluation of discontinuities in rock masses. *Int J Rock Mech Min Sci* 46:194–199
- Lee EM, Jones DKC (2004) *Landslide risk assessment*. Thomas Telford, London, p 454. ISBN 9780727731715
- Li ZH, Huang HW, Xue YD, Yin J (2009) Risk assessment of rockfall hazards on highways. *Georisk* 3:147–154
- Lim M, Petley DN, Rosser NJ, Allison RJ, Long AJ (2005) Digital photogrammetry and time-of-flight laser scanning as integrated approach to monitoring cliff evolution. *Photogramm Rec* 20(110):109–129
- Locat P, Couture R, Leroueil S, Locat S (2006) Fragmentation energy in rock avalanches. *Can Geotech J* 43:830–851
- Lu P, Latham JP (1999) Developments in the assessment of in-situ block size distributions in rock masses. *Rock Mech Rock Eng* 32:29
- Malamud B, Turcotte L, Guzzetti F, Reichenbach P (2004) Landslide inventories and their statistical properties. *Earth Surf Proc Land* 29:687–711
- Mavrouli O, Corominas J (2017) Comparing rockfall scar volumes and kinematically detachable rock masses. *Eng Geol* 219:63–74
- Mavrouli O, Corominas J, Jaboyedoff M (2015) Size distribution for potentially unstable rock masses and in situ rock blocks using LiDAR-generated digital elevation models. *Rock Mech Rock Eng* 48(4):1589–1604
- McSaveny MJ (2002) Recent rockfalls and rock avalanches in Mount Cook National Park, New Zealand. In: Evans SG, DeGraff JV (eds) *Catastrophic landslides: effects, occurrence, and mechanisms*, vol 15 (Rev Eng Geol). Geological Society of America, pp 35–70

- Michoud C, Bazin S, Blikra LH, Derron MH, Jaboyedoff M (2013) Experiences from site-specific landslide early warning systems. *Nat Hazards Earth Syst Sci* 13:2659–2673
- Moya J, Corominas J, Perez-Arcas J, Baeza C (2010) Tree-ring based assessment of rockfall frequency on talus slopes at Solà d'Andorra, Eastern Pyrenees. *Geomorphology* 118:393–408
- Okura Y, Kitahara H, Sammori T, Kawanami A (2000) The effects of rockfall volume on runout distance. *Eng Geol* 58(2):109–124
- Oppikofer T, Jaboyedoff M, Keusen HR (2008) Collapse of the eastern Eiger flank in the Swiss Alps. *Nat Geosci* 1:531–535
- Oppikofer T, Jaboyedoff M, Blikra L, Derron MH (2009) Characterization and monitoring of the Aknes rockslide using terrestrial laser scanning. *Nat Hazards Earth Syst Sci* 9:1643–1653
- Oppikofer T, Jaboyedoff M, Pedrazzini A, Derron MH, Blikra LH (2011) Detailed DEM analysis of a rockslide scar to characterize the basal sliding surface of active rockslides. *J Geophys Res Earth Surf* 116
- Palmström A (2001) Measurement and characterization of rock mass jointing. In: Sharma VI, Saxena K (eds) *In-situ characterization of rocks*. A. A. Balkema publishers
- Palmstrom A (2005) Measurement of and correlations between block size and rock quality designation (RQD). *Tunn Undergr Space Technol* 20:362–377
- Pedrazzini A, Humair F, Jaboyedoff M, Tonini M (2016) Characterisation and spatial distribution of gravitational slope deformation in the Upper Rhone catchment (Western Swiss Alps). *Landslides* 13:259–277
- Pelletier JD, Malamud BD, Blodgett TA, Turcotte DL (1997) Scale-invariance of soil moisture variability and its implications for the frequency-size distribution of landslides. *Eng Geol* 48:254–268
- Perfect E (1997) Fractal models for the fragmentation of rocks and soils: a review. *Eng Geol* 48:185–198
- Petley DN (2012) Landslides and engineered slopes: protecting society through improved understanding. In: Eberhardt E, Froese C, Turner AK, Leroueil S (eds) *Landslides and engineered slopes*, vol 1. CRC Press, London, pp 3–13
- Petley DN, Bulmer MHK, Murphy W (2002) Patterns of movement in rotational and translational landslides. *Geology* 30:719–722
- Picarelli L, Oboni F, Evans SG, Mostyn G, Fell R (2005) Hazard characterization and quantification. In: Hungr O, Fell R, Couture R, Eberhardt E (eds) *Landslide risk management*. Taylor and Francis, London, pp 27–62 ISBN 041538043X
- Poulton MM, Mojtabai N, Farmer IW (1990) Scale invariant behaviour of massive and fragments rock. *Int J Rock Mech Min Sci Geomech Abstracts* 27:219–221
- Priest SD (1993) *Discontinuity analysis for rock engineering*. Chapman and Hall, London, p 473
- Priest SD, Hudson JA (1981) Estimation of discontinuity spacing and trace length using scanline surveys. *Int J Rock Mech Min Sci Geomech Abstracts* 18:183–197
- Riquelme AJ, Abellán A, Tomás R, Jaboyedoff M (2014) A new approach for semi-automatic rock mass joints recognition from 3D point clouds. *Comput Geosci* 68:38–52
- Riquelme AJ, Abellán A, Tomás R (2015) Discontinuity spacing analysis in rock masses using 3D point clouds. *Eng Geol* 195:185–195
- Rochet L (1987) Application des modeles numeriques de propagation a l'etude des eboulements rocheux. *Bull Lab Ponts et Chaussées* 150 (151):84–95
- Rose ND, Hungr O (2007) Forecasting potential rock slope failure in open pit mines using the inverse-velocity method. *Int J Rock Mech Min Sci* 44:308–320
- Rosser N, Lim M, Petley D, Dunning S, Allison R (2007) Patterns of precursory rockfall prior to slope failure. *J Geophys Res* 112: F04014
- Royán MJ, Abellán A, Jaboyedoff M, Vilaplana JM, Calvet J (2014) Spatio-temporal analysis of rockfall pre-failure deformation using Terrestrial LiDAR. *Landslides* 11:697–709
- Royán MJ, Abellán A, Vilaplana JM (2015) Progressive failure leading to the 3 December 2013 rockfall at Puigcerçós scarp (Catalonia, Spain). *Landslides* 12:585–595
- Ruiz-Carulla R, Corominas J, Mavrouli O (2015a) A methodology to obtain the block size distribution of fragmental rockfall deposits. *Landslides* 12(4):815–825
- Ruiz-Carulla R, Corominas J, Mavrouli O (2015b) An empirical approach to rockfall fragmentation. In: Eurock 2015—ISRM European Regional Symposium—the 64th Geomechanics Colloquium, 7–10 October 2015, Salzburg, Austria
- Ruiz-Carulla R, Corominas J, Mavrouli O (2016a) Comparison of block size distribution in rockfalls. In: Aversa S, Cascini L, Picarelli L, Scavia C (eds) *Landslides and engineered slopes: experience, theory and practice*, vol 3. CRC press, pp 1767–1774. ISBN 978-1-138-02991-0
- Ruiz-Carulla R, Matas G, Prades A, Gili JA, Corominas J, Lantada N, Buill F, Mavrouli O, Núñez-Andrés A, Moya J (2016b) Analysis of rock block fragmentation by means of real-scale tests. In: 3rd RSS Rock Slope Stability conference, Lyon 2016, p 2
- Ruiz-Carulla R, Corominas J, Mavrouli O (2017, available online) A fractal fragmentation model for rockfalls. *Landslides*. doi: [10.1007/s10346-016-0773-8](https://doi.org/10.1007/s10346-016-0773-8)
- Saito M (1965) Forecasting the time of occurrence of a slope failure. *Proceedings of the 6th International Conference on Soil Mechanics and Foundation Engineering*. Pergamon Press, Montréal, Oxford, pp 537–541
- Salciarini D, Tamagnini C, Conversini P (2009) Numerical approaches for rockfall analysis: a comparison. In: *Proceedings 18th World IMACS/MODSIM Congress*, Cairns, Australia
- Santana D, Corominas J, Mavrouli O, Garcia-Sellés D (2012) Magnitude-frequency relation for rockfall scars using a Terrestrial Laser Scanner. *Eng Geol* 145–146:50–64
- Selby MJ (1982) *Hillslope materials and processes*. Oxford University Press, New York
- Slob S (2010) Automated rock mass characterisation using 3-D terrestrial laser scanning. Ph.D. thesis, TU Delft. URL: <http://www.narcis.nl/publication/RecordID/oai:tudelft.nl:uuid:c1481b1d-9b33-42e4-885a-53a6677843f6>
- Slob S, Hack R, Turner A K (2002) An approach to automate discontinuity measurements of rock faces using laser scanning techniques. In: Da Gama CD, Sousa LRE (eds) *ISRM EUROCK 2002*, Lisbon, Portugal. ISBN: 972-98781-2-9, pp. 87–94
- Slob S, Hack R, van Knapen B, Kemeny J (2004) Automated identification and characterization of discontinuity sets in outcropping rock masses using 3D terrestrial laser scan survey techniques. In: *Proceedings of the ISRM Regional Symposium EUROCK 2004 & 53rd Geomechanics Colloquy*, Salzburg, pp 439–443
- Soeters R, Van Westen CJ (1996) Slope instability, recognition, analysis and zonation. In: Turner AT, Schuster RL (eds) *Landslides—investigation and mitigation*, Transportation Research Board Special Report No 247. National Academy Press, Washington DC, pp 129–177
- Spang RM, Rautenstrauch RW (1988) Empirical and mathematical approaches to rock fall protection and their practical application. In: Bonnard C (ed) *5th International Congress on Landslides*, vol 2. Lausanne. Balkema, Rotterdam, pp 1237–1243. ISBN 90-6191-838-3
- Stark CP, Hovius N (2001) The characterization of the landslide size distributions. *Geophys Res Lett* 28:1091–1094
- Statham I (1976) A scree slope rockfall model. *Earth Surf Proc Land* 1:43–62

- Stead D, Eberhardt E, Coggan JS (2006) Developments in the characterization of complex rock slope deformation and failure using numerical modelling techniques. *Eng Geol* 83:217–235
- Stock GM, Martel SJ, Collins BD, Harp EL (2012) Progressive failure of sheeted rock slopes: the 2009–2010 Rhombus Wall rock falls in Yosemite Valley, California, USA. *Earth Surf Proc Land* 37:546–561
- Sturzenegger M, Stead D (2009a) Quantifying discontinuity orientation and persistence on high mountain rock slopes and large landslides using terrestrial remote sensing techniques. *Nat Hazards Earth Syst Sci* 9(2):267–287
- Sturzenegger M, Stead D (2009b) Close-range terrestrial digital photogrammetry and terrestrial laser scanning for discontinuity characterization on rock cuts. *Eng Geol* 106:163–182
- Turcotte D (1986) Fractals and fragmentation. *J Geophys Res* 91 (B2):1921–1926
- Turner AK, Jayaprakash GP (2012) Introduction. In: Turner AK, Schuster RL (eds) *Rockfall characterization and control*. Transportation Research Board, National Academy of Sciences, Washington D.C., pp 3–20
- Voight B (1989) A relation to describe rate-dependent material failure. *Science* 243:200–203
- Volkwein A, Schellenberg K, Labiouse V, Agliardi F, Berger F, Bourrier F, Dorren LKA, Gerber W, Jaboyedoff M (2011) Rockfall characterisation and structural protection—a review. *Nat Hazards Earth Syst Sci* 11:2617–2651
- Wang Y, Tonon F (2010) Discrete element modeling of rock fragmentation upon impact in rock fall analysis. *Rock Mech Rock Eng* 44:23–35
- Wehr A, Lohr U (1999) Airborne laser scanning—an introduction and overview. *ISPRS J Photogramm Remote Sens* 54:68–82
- Whalley WB (1984) Rockfalls. In: Brunsten D, Prior DB (eds) *Slope instability*. Wiley, New York, pp 217–256
- Wieczorek GF (2002) Catastrophic rockfalls and rockslides in the Sierra Nevada, USA. In: Evans SG, DeGraff J (eds) *Catastrophic landslides: effects, occurrence and mechanisms*. *Rev Eng Geol*, vol 15. Geological Society of America, pp 165–190
- Wieczorek GF, Morrissey MM, Iovine G, Godt J (1998) *Rock fall Hazards in the Yosemite Valley*. US Geological Survey, Open File Report. 98–467
- Wyllie DC, Mah C (2004) *Rock slope engineering: civil and mining*, 4th edn. SponPress, New York, p 431
- Zhang ZX, Kou SQ, Jiang LG, Lindqvist PA (2000) Effects of loading rate on rock fracture: fracture characteristics and energy partitioning. *Int J Rock Mech Min Sci* 37:745–762

Open Access This chapter is licensed under the terms of the Creative Commons Attribution 4.0 International License (<http://creativecommons.org/licenses/by/4.0/>), which permits use, sharing, adaptation, distribution and reproduction in any medium or format, as long as you give appropriate credit to the original author(s) and the source, provide a link to the Creative Commons license and indicate if changes were made.

The images or other third party material in this chapter are included in the chapter's Creative Commons license, unless indicated otherwise in a credit line to the material. If material is not included in the chapter's Creative Commons license and your intended use is not permitted by statutory regulation or exceeds the permitted use, you will need to obtain permission directly from the copyright holder.

